Hyaluronan Rich Microenvironment in the Limbal Stem Cell Niche Regulates Limbal Stem Cell Differentiation

Tarsis F. Gesteira,[1] Mingxia Sun,[2] Yvette M. Coulson-Thomas,[1] Yu Yamaguchi,[3] Lung-Kun Yeh,[4] Vincent Hascall,[5] and Vivien J. Coulson-Thomas[2]

[1]Universidade Federal de Sao Paulo, Sao Paulo, Brazil
[2]College of Optometry, University of Houston, Houston, Texas, United States
[3]Sanford Children's Health Research Center, Sanford-Burnham Medical Research Institute, La Jolla, California, United States
[4]Department of Ophthalmology, Chang-Gung Memorial Hospital, Chang-Gung University College of Medicine, Linko, Taiwan
[5]Cleveland Clinic, Cleveland, Ohio, United States

Correspondence: Vivien J. Coulson-Thomas, University of Houston, College of Optometry, 4901 Calhoun Road, Houston, TX 77204-2020, USA;
vcoulsonthomas@gmail.com,
vjcoulso@central.uh.edu.

Submitted: June 1, 2017
Accepted: July 31, 2017

Citation: Gesteira TF, Sun M, Coulson-Thomas YM, et al. Hyaluronan rich microenvironment in the limbal stem cell niche regulates limbal stem cell differentiation. *Invest Ophthalmol Vis Sci*. 2017;58:4407–4421. DOI: 10.1167/iovs.17-22326

Purpose. Limbal epithelial stem cells (LSCs), located in the basal layer of the corneal epithelium in the corneal limbus, are vital for maintaining the corneal epithelium. LSCs have a high capacity of self-renewal with increased potential for error-free proliferation and poor differentiation. To date, limited research has focused on unveiling the composition of the limbal stem cell niche, and, more important, on the role the specific stem cell niche may have in LSC differentiation and function. Our work investigates the composition of the extracellular matrix in the LSC niche and how it regulates LSC differentiation and function.

Methods. Hyaluronan (HA) is naturally synthesized by hyaluronan synthases (HASs), and vertebrates have the following three types: HAS1, HAS2, and HAS3. Wild-type and HAS and TSG-6 knockout mice—*HAS1*$^{-/-}$;*HAS3*$^{-/-}$, *HAS2*$^{\Delta/\Delta CorEpi}$, *TSG-6*$^{-/-}$—were used to determine the importance of the HA niche in LSC differentiation and specification.

Results. Our data demonstrate that the LSC niche is composed of a HA rich extracellular matrix. *HAS1*$^{-/-}$;*HAS3*$^{-/-}$, *HAS2*$^{\Delta/\Delta CorEpi}$, and *TSG-6*$^{-/-}$ mice have delayed wound healing and increased inflammation after injury. Interestingly, upon insult the HAS knock-out mice upregulate HA throughout the cornea through a compensatory mechanism, and in turn this alters LSC and epithelial cell specification.

Conclusions. The LSC niche is composed of a specialized HA matrix that differs from that present in the rest of the corneal epithelium, and the disruption of this specific HA matrix within the LSC niche leads to compromised corneal epithelial regeneration. Finally, our findings suggest that HA has a major role in maintaining the LSC phenotype.

Keywords: limbal stem cells, hyaluronan, corneal epithelial cells, stem cell niche

The ocular surface is composed of the cornea surrounded by the conjunctiva, and the transition between these is the limbus. The cornea, conjunctiva, and limbus form a continuous epithelial layer. Previous studies provide evidence that the cornea contains a stem cell niche at the basal epithelial layer of the limbus.[1,2] Limbal stem cells (LSCs), located in the basal layer of the corneal epithelium in the corneal limbus, have a vital role in maintaining the cornea. LSCs have a high capacity of self-renewal with increased potential for error-free proliferation and poor differentiation.[3–6] LSCs also have a long cell cycle, small cell size, high nuclear to cytoplasm ratio, and asymmetric division.[7] After cell division, one daughter cell maintains the LSC stemness while the other daughter cell becomes a transient amplifying cell (TAC), with increased proliferative potential.[8–11] TACs migrate out of the stem cell niche and ultimately differentiate into corneal epithelial cells.[9] LSCs are required for reconstituting the corneal epithelium after injury and also have an important role in preventing conjunctival epithelial cells from migrating onto the surface of the cornea. Moreover, limbal stem cell transplantation is capable of restoring the eyesight to a severely damaged ocular surface resulting in rapid corneal re-epithelialization without persistent erosions. Currently, limbal stem cell transplantation is a common surgical procedure that is carried out around the world.[12–16] In humans, the corneoscleral limbus has a series of radially oriented ridges, namely the palisades of Vogt, where the LSCs are located.[17,18] LSCs express various stem cell markers, such as cytokeratin 15 (K15), ΔNp63α, and ABCG2, and lack differentiated corneal epithelial markers such as cytokeratin 3 and cytokeratin 12 (K12).[9,19–23]

Limbal stem cell deficiency (LSCD) is a condition caused by damage or loss of LSCs. LSCD is a serious medical condition that leads to corneal opacification, inflammation, vascularization, and severe pain and may lead to the complete loss of vision.[9,24,25] A hallmark of LSCD is the migration of conjunctival cells onto the cornea leading to conjunctivalization, which results in severe vision loss and requires corneal transplantation.[3,26] Substantial research has been dedicated to developing new therapeutic approaches for treating LSCD. An emerging surgical approach is the transplantation of LSCs expanded ex vivo from either the residual LSCs of a patient or from a human leukocyte antigen–matched donor.[9,27–29] However, many LSCD patients present nonresolving inflammation, which limits the success of corneal and LSC transplantation.[30–32] Studies have

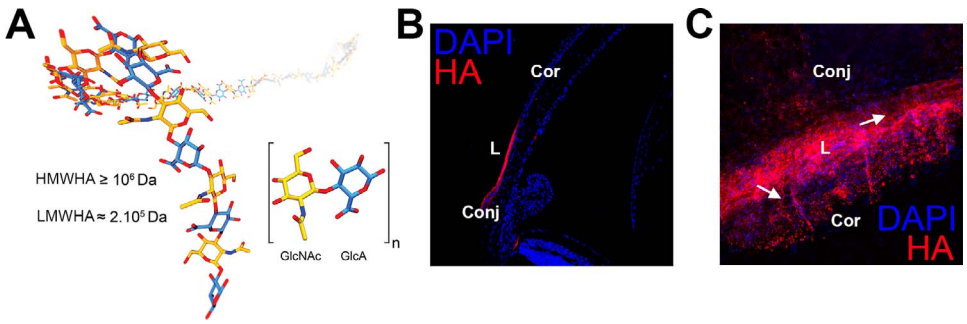

Figure 1. Chemical structure of HA (**A**). HA staining in mouse corneal sections (**B**) and whole mount (**C**) revealing that HA is present solely in the corneal limbal region (L) and not present in the peripheral (Cor) or central cornea. Weak HA staining is present in the conjunctiva (Conj) close to the limbal region. HA was stained in the corneas of wild-type mice using biotinylated link protein (*red*). HA cables can be seen extending through the corneal limbus and into the peripheral cornea (*arrows*). Nuclei were counterstained with DAPI (*blue*).

shown the great therapeutic potential of amniotic membrane transplantation for treating LSCD. Recently, the Tseng group showed that a hyaluronan (HA) complex was responsible for the efficacy of amniotic membrane treatment.[30] This group also went on to show that this HA complex in the amniotic membrane actively suppresses inflammation, making it an attractive candidate for the development into treatment for LSCD.[30]

HA is a ubiquitous component of the extracellular matrix that is enriched during early stages of development and disease. HA is a high molecular weight glycosaminoglycan composed entirely of repeating disaccharide units of D-glucuronic acid and N-acetylglucosamine, which are alternately linked by β-1,3- and β-1,4-glycosidic bonds (Fig. 1A).[33–35] HA is naturally synthesized by a class of integral membrane proteins, hyaluronan synthases (HASs), of which vertebrates have the following three types: HAS1, HAS2, and HAS3.[36] Studies have shown that primarily the following two forms of HA exist: high molecular weight HA (HMWHA) of approximately 2,000 kDa and low molecular weight HA (LMWHA) of approximately 200 kDa. HMWHA has anti-inflammatory effects and is primarily correlated with tissue integrity, whereas LMWHA has proinflammatory effects and is primarily correlated with pathogenesis.[37–41] We have recently shown that HA matrices present around umbilical cord mesenchymal stem cells actively suppress inflammatory cells, enabling these stem cells to evade host xenograft rejection.[42] We have also recently shown that a specific HA matrix is up-regulated after brain and spinal cord injury and forms a principal constituent of the glial scar.[43] Therefore, targeting the HA content during pathogenesis, including injury, inflammatory disorders, cardiovascular disease, and cancer, is becoming an attractive strategy for intervention. In recent years, many studies have demonstrated that during inflammatory processes Inter-α-Inhibitor (IαI, also known as ITI) expressed by the liver infiltrates the site of inflammation where it participates in the assembly of a specific anti-inflammatory matrix.[44,45] Hascall and Salustri et al. discovered that TNFα-stimulated gene 6 (TSG-6) transfers heavy chains (HCs) from IαI to HA, forming a specialized HC-HA/TSG-6 matrix.[46–48] Since this pioneering work, many groups have shown that variations of this HA matrix are monocyte-adhesive and are found in most, if not all, inflammatory processes.[49–52] Modified HA matrices bind inflammatory cells, and the interaction of these cells with the HA matrices modulates their responses, which are central to pathological inflammation.[49,50] Pentraxin 3 (PTX3) and spliced variants of versican can also be present in this modified matrix, forming a HC-HA/TSG-6/PTX3/versican matrix with anti-inflammatory properties.[53–55] Interestingly, the amniotic membrane and umbilical cord have been shown to be extrahepatic tissues capable of secreting IαI.[42,56]

Stem cells throughout the body require a highly specialized stem cell niche, which supports the stem cell phenotype. To date limited research has focused on determining the composition of the corneal LSC niche, and, more important, the role this specific stem cell niche may have in LSC differentiation and function. Therefore, the purpose of this study was to characterize the composition of the LSC niche and determine the role of the LSC niche in maintaining LSCs. Our results show that the LSC niche is composed of a HA rich matrix. Using knock-out mice for the different HAS enzymes, our results indicate that the HA matrix is necessary for maintaining the LSC phenotype. Characterization of the role of the HA matrix in the corneal LSC niche opens possible new therapeutic avenues for treating LSCD by re-establishing the LSC niche to provide the environment necessary to support LSCs.

Materials and Methods

Animal Maintenance

Mouse Strains and Genotyping. Transgenic mouse lines K14-rtTA (stock number 008099)[57] and tetO-cre (stock number 006224)[58] from The Jackson Laboratory were used (Bar Harbor, ME, USA). Floxed *HAS2* mice, namely *HAS2*$^{flox/flox}$,[59] *Null TSG-6*,[60] hereafter referred to as *TSG-6*$^{-/-}$ mice, and combined *HAS1*[61] and *HAS3 null*[62] mice, hereafter referred to as *HAS1*$^{-/-}$;*HAS3*$^{-/-}$ mice, were used. Compound K14-rtTA, tetO-cre, and *HAS2*$^{flox/flox}$ transgenic mice were generated by mating. The mice were bred and housed in a temperature-controlled facility with an automatic 12-hour light–dark cycle at the Animal Facility of the University of Houston. Experimental procedures for handling the mice were approved by the Institutional Animal Care and Use Committee, University of Houston. All animal procedures adhered to the ARVO Statement for the Use of Animals in Ophthalmic and Vision Research. The identification of each transgene allele was determined by PCR genotyping with tail DNA. Administration of doxycycline chow was used to induce K14-driven persistent and irreversible excision of HAS2 in the corneal epithelium (CorEpi) of tetratransgenic mice (*K14-rtTA;TC;HAS2*$^{flox/flox}$), generating *HAS2*$^{\Delta/\Delta CorEpi}$. Transgenic mice at postnatal day 7 (P7) or P21 were fed with doxycycline chow (1 g of doxycycline/kg of chow; Custom Animal Diets LLC, Bangor, PA, USA) ad libitum. Control animals *TSG-6*$^{+/-}$, *K14-rtTA;HAS2*$^{flox/flox}$ littermates, and C57 black 6 (C57BL/6J) mice were used in all experiments, and all yielded comparable results. In most figures, solely results from the C57BL/6J mice are displayed and referred to as wild-type.

Debridement Wound for RNA Extraction. Corneal epithelial debridement wounds (1.5 mm in diameter) were done on wild-type mice. The mice were anesthetized by intraperitoneal injection of ketamine hydrochloride (80 mg/kg) and xylazine (10 mg/kg). The corneal wound area was demarcated with a 1.5 mm-diameter biopsy punch, and the epithelial debridement wound was done with an AlgerBrush II (Alger Company, Inc., Lago Vista, TX, USA). Thereafter, the debrided cells were removed by washing with PBS and a sponge swab. The eyeballs were collected 2, 4, and 8 hours after debridement wounding and placed in Invitrogen RNA*later* Stabilization Solution (Thermo Fisher Scientific, Wilmington, DE, USA). To analyze HAS expression in uninjured corneas, the mice (0 hours) were euthanized by CO_2 inhalation. Epithelial cells in the central cornea were removed as mentioned previously, and the corneas were immediately placed in Invitrogen RNA*later* Stabilization Solution. Five eyeballs were used for each experimental point.

RNA Extraction and Real-Time PCR Analysis. The eyeballs were dissected and the corneas removed for RNA extraction. mRNA was extracted using the PureLink RNA Mini Kit (Ambion, Life Technologies, Carlsbad, CA, USA), according to the manufacturer's instructions. cDNA was synthesized using SuperScript III First-Strand (Invitrogen), according to the manufacturer's instructions. The primer combination used for qPCR analysis of *HAS1* was 5′-CTATGCTACCAAGTATACCTCG-3′ and 5′-TCTCGGAAGTAAGATTTGGAC-3′, of *HAS2* was 5′-CGGTCGTCTCAAATTCATCTG-3′ and 5′-ACAATGCATCTTGTT CAGCTC-3′, of *HAS3* was 5′-GATGTCCAAATCCTCAACAAG-3′ and 5′-CCCACTAATACATTGCACAC-3′,[63] and of *TSG-6* was forward: 5′-ACGATGTCCACGGCTTTGTAGG-3′ and reverse: 3′-GACGCATCACAAACTTCAAGG-5′. Real-time PCR was done using SyberGreen and analyzed using a Biorad CFX96 C1000 Thermal Cycler (Biorad, Hercules, CA, USA). For data analysis, the $2^{-\Delta Ct}$ method was used, and data were normalized to the reference genes 40S ribosomal protein S29 (*RPS29*) and glyceraldehyde-3-phosphate dehydrogenase (*GADPH*) using the 7500 Real-Time PCR System's software and yielded comparable results. The data normalized to *RPS29* are presented. The specificity of the amplified products was analyzed through dissociation curves generated by the equipment yielding single peaks and subsequently confirmed by sequencing. Negative controls were used in parallel to confirm the absence of any form of contamination in the reaction.

Ex Vivo Debridement Wound. Ex vivo corneal epithelial debridement wounds (1.5 mm in diameter) were done on wild-type, *HAS1*$^{-/-}$;*HAS3*$^{-/-}$, and *HAS2*$^{\Delta CorEpi}$ mice as mentioned previously. The mice were euthanized by CO_2 inhalation and transported to a laminar flow hood prior to the injury. The wounded area was determined immediately (0 hours), and at 6, 12, and 24 hours after the injury by placing 20 µL of a 1 mg/mL fluorescein solution on the cornea. The eyeball was then washed with PBS and placed with the cornea facing upwards in an eyeball insert (designed at the University of Houston) for imaging the corneal surface under a Zeiss Discovery.V12 Stereo Microscope (Zeiss, Oberkochen, Germany). The eyeball was then removed from the insert and, after washing away any excess fluorescein, was placed back in the insert with the cornea facing upward and incubated in complete media at 37°C and 5% CO_2. The wounded area was measured using ImageJ software (http://imagej.nih.gov/ij/; provided in the public domain by the National Institutes of Health, Bethesda, MD, USA). Eyeballs were fixed at 12 and 24 hours in 4% buffered paraformaldehyde for analysis by immunohistochemistry. At least five mice were used for each experimental point.

Alkali Burn. The alkali burn model in this study spares the corneal epithelial limbal region. In preparation for the alkali burn, the mice were provided with carprofen gel packs ad libitum 24 hours before the alkali burn procedure. Prior to the alkali burn, the mice were anesthetized by intraperitoneal injection of ketamine hydrochloride (80 mg/kg) and xylazine (10 mg/kg), and eyes were topically anesthetized with a drop of proparacaine. The alkali burn protocol sparing the epithelial limbal region was done as previously described.[42] In short, contained alkali burns were produced by placing circular 3MM chromatography paper (1-mm diameter; Whatman, Little Chalfont, Buckinghamshire, United Kingdom) soaked in 0.1 M sodium hydroxide onto the central cornea for 1 minute and 15 seconds. Subsequently, the eyes were continuously washed with sterile PBS for 1 minute. This contained alkali burn protocol avoids damaging the limbal stem cells, which allows comparisons of the effects of HA depletion on suppression of inflammation and regeneration of a transparent cornea without depleting LSCs through the alkali burn procedure itself. Finally, terramycin ointment was topically administered to the eyes, and the animals were placed on a warming pad. A total of 20 mice were used for each experimental point, and 12 were processed for histological analysis and eight for whole-mount staining.

Histochemistry. Eyeballs were fixed for 30 minutes in 2% buffered paraformaldehyde, washed five times with PBS, sequentially dehydrated, immersed in paraffin overnight, and subsequently mounted. The blocks were sectioned at 5 µm, and the sections collected on poly-L-lysine-treated slides. Upon use, the paraffin sections were washed with xylene to remove excess paraffin and then rehydrated. Subsequently, the sections were stained with hematoxylin and eosin. A Periodic-Schiff kit (395B-1KT, Sigma-Aldrich Corp., St. Louis, MO, USA) was used for detecting goblet cells in the corneas of *HAS2*$^{\Delta CorEpi}$ mice according to the manufacturer's instructions. In short, a drop of periodic acid solution was placed on each tissue section and left at room temperature for 5 minutes and then washed with double distilled water. Subsequently, a drop of Schiff's reagent was placed on each tissue for 15 minutes at room temperature and then rinsed. The nuclei were then counterstained with hematoxylin for 90 seconds at room temperature and slides rinsed in running water. The sections were washed, dehydrated, and mounted in Permount (ThermoFisher Scientific). Images were captured using a Nikon Eclipse E800 microscope (Shinagawa, Tokyo, Japan) coupled to a Zeiss AxioCam ICc5 camera and images analyzed using AxioVision (Zeiss).

Immunohistochemistry. Paraffin sections were heated at 65°C for 30 minutes and subsequently washed with xylene to remove excess paraffin and then rehydrated. Unspecific protein binding sites were blocked with 5% fetal bovine serum (FBS). Sections were then incubated with the primary antibodies rabbit anti-Krt14 (PRB-155P; Covance, Princeton, NJ, USA), rabbit anti-Krt14 (PA5-16722; ThermoFisher Scientific), rabbit anti-Krt12 (ab185627; Abcam, Cambridge, MA, USA), mouse anti-Krt15 (LHK15; ThermoFisher Scientific), goat anti-ionized calcium-binding adapter molecule 1 (*Iba1*) (ab5076; Abcam), and rat anti-F4/80 (ab6640; Abcam). Sections were washed and incubated with appropriate secondary donkey antibodies conjugated with Alexa Fluor 488 or Alexa Fluor 555 for 1 hour at 18°C. For HA staining, corneas were incubated with biotinylated HA binding protein (HABP-385911; Millipore, Billerica, MA, USA) followed by NeutrAvidin Alexa 555 (Life Technologies, Carlsbad, CA, USA). For whole-mount staining, corneas were excised from enucleated eyeballs, treated for 15 minutes in 0.1% sodium borohydrate, and the unspecific protein binding sites were blocked with 5% FBS for 24 hours with shaking. The corneas were then incubated with a primary antibody, rabbit anti-Krt12, rabbit anti-Krt14, mouse anti-Krt15, rat anti-F4/80 (ab6640; Abcam) or mouse anti-α-smooth muscle actin (SMAα; clone 1A4; Sigma-Aldrich), for 24 hours followed by the secondary donkey antibodies conjugated with Alexa

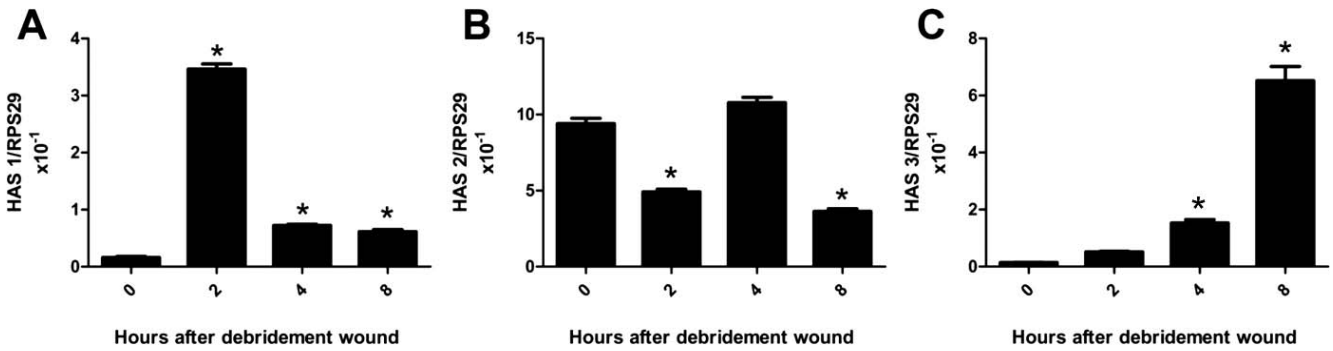

FIGURE 2. HAS1, HAS2, and HAS3 mRNA expressions after corneal debridement wounds. Wild-type mice were subjected to corneal debridement wounds and corneas harvested immediately (0), and at 2, 4, and 8 hours after injury. RNA was extracted and subjected to real-time PCR analysis for HAS1 (**A**), HAS2 (**B**), and HAS3 (**C**) mRNA expression. $^*P \leq 0.05$ compared to 0 hours.

Fluor 488 or Alexa Fluor 555. For HA staining, the corneas were incubated with HA binding protein for 8 hours at 4°C followed by NeutrAvidin Alexa 555. The sections and tissues were then washed and nuclei stained with 4′,6-diamidino-2-phenylindole (DAPI; Sigma-Aldrich). The sections were mounted in Prolong Gold (Molecular Probes, Eugene, OR, USA) and corneas mounted in Fluoromount-G (Electron Microscopy Sciences, Hatfield, PA, USA). Images were captured using a ZEISS LSM 800 Confocal microscope with Airyscan and analyzed using the Zen Image software (Zeiss). Macrophages and SMAα positive ($SMA\alpha^+$) cells were counted by two separate investigators in a blinded manner. Secondary isotype controls were done with a rabbit IgG isotype control (ab37415; Abcam) and mouse IgG1 isotype control (ab91353; Abcam) in place of the primary antibody and did not yield any significant staining (results not shown).

Transmission Electron Microscopy. Cornea samples were fixed in 0.1 M cacodylate buffer (pH 7.4) containing 2% glutaraldehyde overnight. Samples were refixed in 1% osmium tetroxide for 1 hour at 48°C, washed in 0.1 M cacodylate buffer (pH 7.4) three times for 10 minutes each, dehydrated in a graded ethanol series, and embedded in Epon 812 epoxy resin (Polysciences, Inc., Warrington, PA, USA). Ultrathin 50-nm sections were obtained and stained with uranyl acetate and lead citrate, and the images captured with a Hitachi 7500 transmission electron microscope (Hitachi, Tokyo, Japan) equipped with an Advanced Microscopy Techniques (AMT) digital camera. At least three eyeballs were used for each experimental point.

In Vivo Confocal Microscopy. Analyses of corneal structures and stromal haze were done with a Heidelberg Retinal Tomograph-HRTIII Rostock Cornea Module (Heidelberg Engineering, Inc., Heidelberg, Germany) according to the manufacturer's instructions. Briefly, GenTeal Gel (Novartis Pharmaceuticals Corp., East Hanover, NJ, USA) was applied to both the eyeball and the tip of the Heidelberg Retinal Tomograph-HRTIII Rostock Cornea Module objective as immersion fluid.[64] Subsequently, a series of 40 images were collected from the corneal epithelium to the endothelium as a continuous *z*-axis scan through the entire cornea at 2 μm to 3 μm increments. All mice used in this study were analyzed by in vivo confocal microscopy prior to euthanasia.

Fluorescein Staining. A drop of Flura-Safe Fluorexon Disodium & Benoxinate Hydrochloride Ophthalmic Solution 0.35%/0.4% (Apollo Ophthalmics, Newport Beach, CA, USA) was placed over the mouse eyeballs for 1 minute, and the excess removed with PBS washes. The eyeballs were imaged using a Zeiss Discovery.V12 Stereo Microscope (Zeiss). At least seven eyeballs were used for each experimental point.

Statistical Analysis

All values are presented as means ± standard deviation of the mean. The difference between two groups was compared by Student's *t*-test. $P \leq 0.05$ was considered to be statistically significant. Statistical analysis was done using the GraphPad Prism version 7 software package (GraphPad Software, San Diego, CA, USA).

RESULTS

Detection of HA in the LSC Niche

The composition of the LSC niche was investigated by immunostaining the corneas of C57BL/6J mice for numerous extracellular matrix components. Our objective was to find molecules differentially expressed in the limbal region when compared with the rest of the corneal epithelium. Of all the molecules investigated, we found that HA was primarily expressed in the LSC niche (Figs. 1B, 1C). HA staining was present in all the epithelial layers in the corneal limbal region (Fig. 1B). The HA forms a net-like network within the corneal limbus and cable-like structures (arrows) that extend from the limbus into the peripheral cornea (Fig. 1C). The specificity of HA expression to the limbal stem cell niche led us to investigate the role of HA in maintaining the limbal stem cell niche.

Analysis of the HAS1, HAS2, and HAS3 Expression Profiles

Three HA synthases, HAS1, HAS2, and HAS3, can synthesize HA. To date no studies have assessed which of the HAS enzymes are expressed in the corneal tissue. Therefore, RNA was extracted from uninjured corneas (referred to as 0 hours) and from corneas at 2, 4, and 8 hours after a debridement wound and analyzed by qPCR to quantify the expression of HAS1, HAS2, and HAS3. To ensure that RNA was extracted solely from the corneal limbus in the uninjured mice, the mice were euthanized, and an Algerbrush was then used to remove the central epithelial cells. Therefore RNA was extracted from limbal epithelial cells and not from corneal epithelial cells. Interestingly, our results show that all three HAS mRNAs are expressed in the cornea (Fig. 2). The uninjured cornea presents all three mRNAs, with HAS2 mRNA expression much higher, indicating that in the healthy cornea the LSC niche may be maintained by all three HAS enzymes but with HAS2 likely to be predominant. Two hours after a debridement wound to the corneal epithelium, HAS1 mRNA

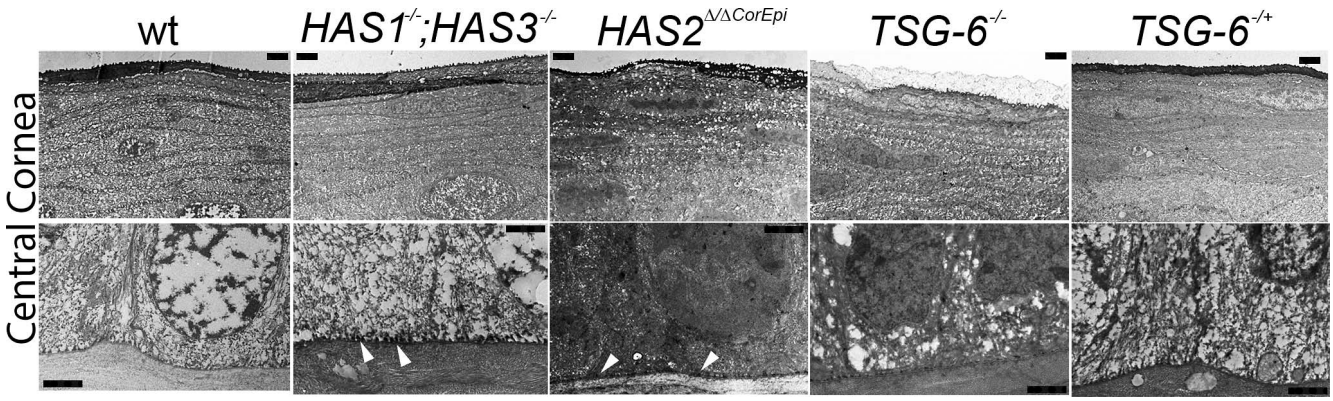

FIGURE 3. The ultra-structures of *HAS1*$^{-/-}$;*HAS3*$^{-/-}$, *HAS2*$^{\Delta/\Delta CorEpi}$, *TSG-6*$^{-/-}$, *TSG-6*$^{-/+}$, and wild-type mouse central corneas were analyzed by electron microscopy. *HAS1*$^{-/-}$;*HAS3*$^{-/-}$ and *HAS2*$^{\Delta/\Delta CorEpi}$ mice, but not *TSG-6*$^{-/-}$ mice, have an increase in the number and size of adhesion complexes (*white arrows*) between basal epithelial cells and the basement membrane when compared with the wild-type mice. *Scale bars*: 2 μm.

expression increased by 19-fold while HAS2 mRNA decreased 0.5-fold (Figs. 2A, 2B). These results provided evidence that immediately after injury HAS1 may be primarily responsible for the synthesis of HA. At 4 hours after injury, HAS1 mRNA expression dropped and remained the same at 8 hours; however, the expression levels at 4 and 8 hours were still ~4-fold higher than at 0 hours. On the other hand, HAS3 mRNA expression gradually increased over time after injury, ~3-fold at 2 hours, ~9.5-fold at 4 hours, and ~44-fold at 8 hours compared to 0 hour (Fig. 2C). HAS2 mRNA expression decreased at 2 hours by 50%, returning to original levels at 4 hours, and dropping again to 50% at 8 hours (Fig. 2B). Interestingly, the two drops in HAS2 mRNA expression coincided with the major peaks of HAS1 mRNA (2 hours) and HAS3 mRNA (8 hours) expressions, respectively. Thus, HAS2 mRNA expression seemed to follow a compensatory mechanism after injury, where its expression was decreased when HAS1 mRNA and HAS3 mRNA expressions were elevated. These results indicated that all the HASs may be required for maintaining the corneal epithelium and also after injury. Thus, to establish the role of HA in the LSC niche in the mouse cornea, we obtained transgenic strains for the three different HASs. Given that TSG-6 catalyzes the transfer of HCs onto the HA chains forming a HC-HA/TSG-6 matrix in injured tissues, we also obtained *TSG-6*$^{-/-}$ mice.

Analysis of Corneas From *HAS1*$^{-/-}$;*HAS3*$^{-/-}$, *HAS2*$^{\Delta CorEpi}$, and *TSG-6*$^{-/-}$ Mice

To establish the role of the HA matrix in corneal development and homeostasis, *HAS1*$^{-/-}$;*HAS3*$^{-/-}$, *HAS2*$^{\Delta CorEpi}$, *TSG-6*$^{-/-}$, and wild-type mice were used. *HAS1*$^{-/-}$;*HAS3*$^{-/-}$, *HAS2*$^{\Delta CorEpi}$ (induced at P7 and P21), and *TSG-6*$^{-/-}$ mice presented no obvious corneal macroscopic defects. By histology analysis using hematoxylin and eosin (H&E) staining, the corneas from *HAS1*$^{-/-}$;*HAS3*$^{-/-}$ and *HAS2*$^{\Delta CorEpi}$ mice (induced at P21) presented a decrease in the number of epithelial cell layers (Supplementary Fig. S1). The ultrastructure of the corneas was also analyzed by electron microscopy, and images of the basal and superficial cells were shown (Fig. 3). No obvious morphological changes were observed in the corneas of the heterozygous *TSG-6*$^{-/+}$ mice (Fig. 3). However, subtle changes were observed in the morphology of corneal epithelial basal cells of *HAS1*$^{-/-}$; *HAS3*$^{-/-}$ and *HAS2*$^{\Delta CorEpi}$ mice (Fig. 3). The cornea is formed of an epithelial cell layer, a stroma, and an endothelial cell layer. A highly specialized basement membrane is located between the corneal epithelial basal cells and the stroma. This specialized basement membrane is necessary for anchoring epithelial cells to the stroma and provides a substrate for the migration of epithelial cells. Adhesion complexes between the basal cells and the basement membrane can be seen in higher magnification electron microscopy images (Fig. 3, white arrows). Interestingly, the size and number of adhesion complexes between the basal epithelial cells and the basement membrane was increased in the *HAS1*$^{-/-}$;*HAS3*$^{-/-}$ and *HAS2*$^{\Delta CorEpi}$ mice, and there was an increased number of adhesion complexes in the *TSG-6*$^{-/-}$ mice when compared with the wild-type mice. No obvious changes were observed in the stroma of the *HAS1*$^{-/-}$;*HAS3*$^{-/-}$, *HAS2*$^{\Delta CorEpi}$, or *TSG-6*$^{-/-}$ mice.

Role of HA and TSG-6 in Corneal Inflammation

TSG-6 and HA matrices have a well-established role in inflammation; therefore, the effect of HA and TSG-6 on the infiltration and resolution of inflammatory responses was analyzed using alkali burn in *HAS1*$^{-/-}$;*HAS3*$^{-/-}$, *HAS2*$^{\Delta CorEpi}$ (induced at P7), *TSG-6*$^{-/-}$, and wild-type mice. Corneal integrity and the inflammatory response were evaluated 2 weeks after alkali burn. At this time, wild-type mice presented a fully healed corneal epithelium with ~7 to 8 cell layers, whereas *HAS1*$^{-/-}$;*HAS3*$^{-/-}$ and *HAS2*$^{\Delta CorEpi}$ mice presented disorganized corneal epithelial layers, making it difficult to evaluate the number of cell layers (Fig. 4A). Moreover, *HAS1*$^{-/-}$; *HAS3*$^{-/-}$ and *HAS2*$^{\Delta CorEpi}$ basal cells presented a loss of the columnar morphology (Fig. 4A). Interestingly, Periodic-Schiff staining revealed that *HAS2*$^{\Delta CorEpi}$ mice present primarily goblet cells in the peripheral cornea (Figs. 4B, 4C) and a few goblet cells in the central cornea (Fig. 4D). *HAS2*$^{\Delta CorEpi}$ mice also presented macrophages in the central and peripheral corneas detected by anti-F4/80 and anti-Iba1 staining (Figs. 4E, 4F, respectively). The corneal epithelium of *TSG-6*$^{-/-}$ mice appeared to be thinner than that of wild-type mice, and there was slight disorganization of the epithelial cell layers; however, this was not as significant as that seen with *HAS1*$^{-/-}$;*HAS3*$^{-/-}$ and *HAS2*$^{\Delta CorEpi}$ mice. The ultrastructure of the corneas 2 weeks after alkali burn was also analyzed by electron microscopy, and images of the basal and superficial cells were shown (Fig. 5). The ultrastructure of the wild-type alkali burn–treated cornea resembled that of the uninjured cornea (Fig. 3). Therefore, these corneas have fully healed from the alkali burn (Fig. 5). However, there were significant changes in the morphology of *HAS1*$^{-/-}$;*HAS3*$^{-/-}$ and *HAS2*$^{\Delta CorEpi}$ mouse corneas. Limited adhesion complexes were found between the basal epithelial cells and the basement membrane of *HAS1*$^{-/-}$;*HAS3*$^{-/-}$ mice (Fig. 5).

Investigative Ophthalmology & Visual Science

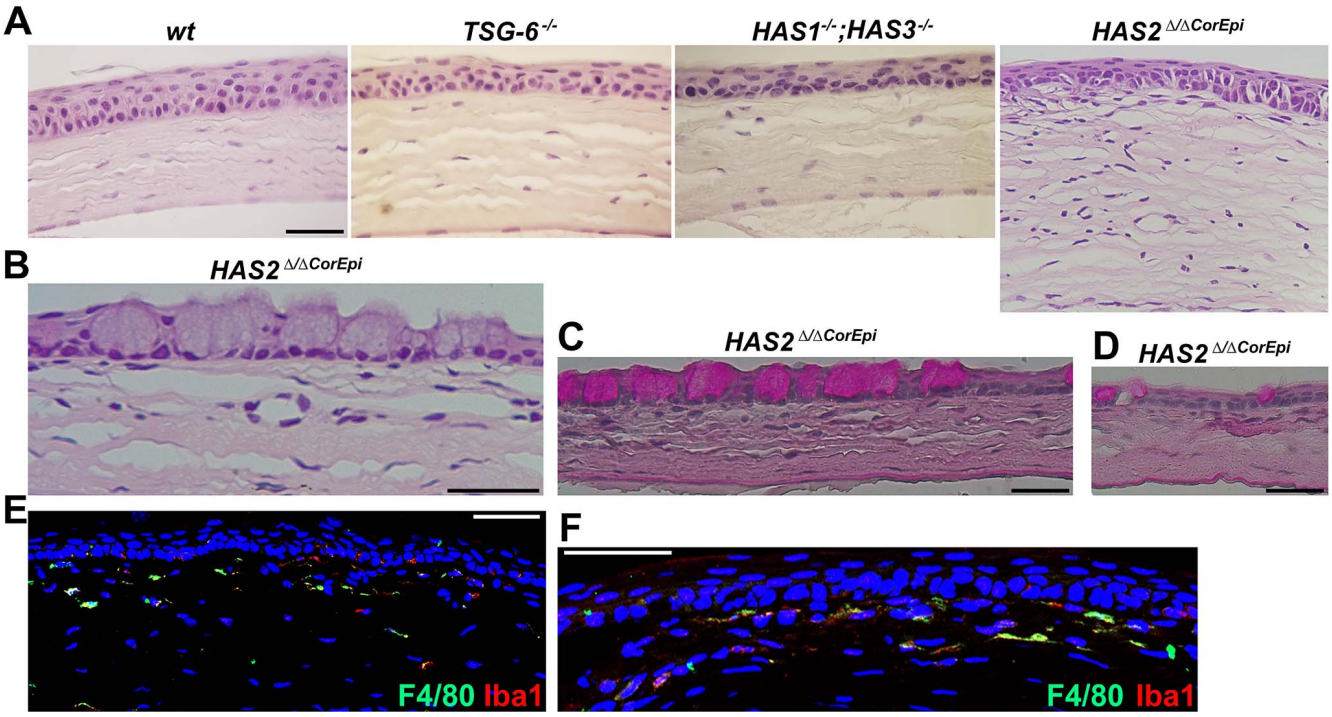

Figure 4. Histological analysis of *HAS1*$^{-/-}$;*HAS3*$^{-/-}$, *HAS2*$^{\Delta/\Delta CorEpi}$, *TSG-6*$^{-/-}$, and wild-type mouse corneas after alkali burn. Sections from corneas of *HAS1*$^{-/-}$;*HAS3*$^{-/-}$, *HAS2*$^{\Delta/\Delta CorEpi}$, *TSG-6*$^{-/-}$ and wild-type mice 2 weeks after an alkali burn were stained with H&E. Images are from the central cornea of all mice (**A**) and from the peripheral cornea of *HAS2*$^{\Delta/\Delta CorEpi}$ mice (**B**). *HAS1*$^{-/-}$;*HAS3*$^{-/-}$ and *HAS2*$^{\Delta/\Delta CorEpi}$ mice show unorganized corneal epithelium, and *HAS2*$^{\Delta/\Delta CorEpi}$ mice present inflammatory cells within the corneal stroma. Sections from *HAS2*$^{\Delta/\Delta CorEpi}$ mice 2 weeks after alkali burn were also stained with Periodic-Schiff, revealing goblet cells (*pink*) in the peripheral cornea (**C**) and central cornea (**D**). Sections from *HAS2*$^{\Delta/\Delta CorEpi}$ mice 2 weeks after alkali burn were stained with anti-F4/80 (*green*), Iba1 (*red*), and DAPI (*blue*) in the central cornea (**E**) and peripheral cornea (**F**). *Scale bars*: 50 μm.

Moreover, the epithelial cells of these mice were unable to form strong cell–cell and cell–matrix adhesion complexes, and after electron microscopy processing there were significant gaps between the epithelial cells and between the epithelial cells and the basement membrane (black arrows, Fig. 5). *HAS2*$^{\Delta CorEpi}$ mice presented basal cells with an uneven cell shape, and the cell membranes presented ridges throughout the corneal epithelium. The *HAS2*$^{\Delta CorEpi}$ basal cells presented deep ridges (white and black arrows in Fig. 5, Supplementary Fig. S2). The reduction in the number of epithelial layers in the corneas of *HAS1*$^{-/-}$;*HAS3*$^{-/-}$ and *HAS2*$^{\Delta CorEpi}$ mice was also evident through electron microscopy analysis. Electron microscopy data suggested that *HAS1*$^{-/-}$;*HAS3*$^{-/-}$ and *HAS2*$^{\Delta CorEpi}$ mice lacked epithelial basal cells and had a reduced number of squamous cell layers when compared with wild-type mice (Fig. 5).

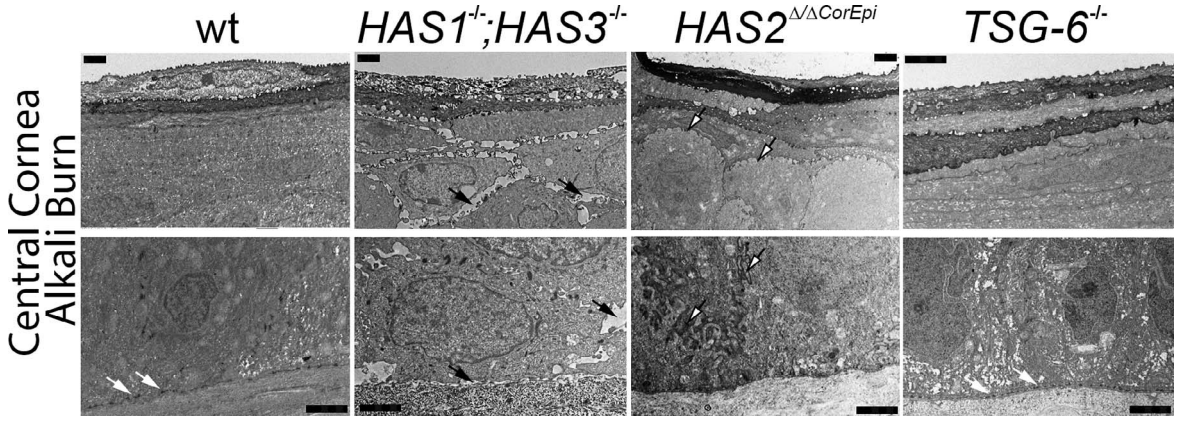

Figure 5. The ultra-structure of *HAS1*$^{-/-}$;*HAS3*$^{-/-}$, *HAS2*$^{\Delta/\Delta CorEpi}$, *TSG-6*$^{-/-}$, and wild-type mouse corneas 2 weeks after alkali burn. The ultra-structure of corneas from *HAS1*$^{-/-}$;*HAS3*$^{-/-}$, *HAS2*$^{\Delta/\Delta CorEpi}$, *TSG-6*$^{-/-}$, and wild-type mice were analyzed by electron microscopy 2 weeks after alkali burn. *HAS1*$^{-/-}$;*HAS3*$^{-/-}$ mice show disrupted cell-cell and cell-basement membrane adhesion complexes, which are clearly seen in control and *TSG-6*$^{-/-}$ mice (*white arrows*). Moreover, *HAS1*$^{-/-}$;*HAS3*$^{-/-}$ epithelial cells are unable to form strong cell-cell and cell-matrix adhesion complexes, and after electron microscopy processing there are significant gaps between the epithelial cells and between the epithelial cells and basement membrane (*black arrows*). *HAS2*$^{\Delta/\Delta CorEpi}$ mice basal cells have an uneven cell shape, and the membranes present ridges (*black and white arrows*). *Scale bars*: 2 μm.

Investigative Ophthalmology & Visual Science

Corneal inflammation was initially assessed using fluorescein to verify the barrier function of wild-type, *HAS1*$^{-/-}$;*HAS3*$^{-/-}$, *HAS2*$^{\Delta CorEpi}$, and *TSG-6*$^{-/-}$ mouse corneas 2 weeks after alkali burn (Fig. 6A). Wild-type and *TSG-6*$^{-/-}$ mice did not present any corneal fluorescein staining, indicating that there was no breach of the barrier function between the epithelial cells (Fig. 6A). However, *HAS1*$^{-/-}$;*HAS3*$^{-/-}$ and *HAS2*$^{\Delta CorEpi}$ (induced at P7) mice presented dense fluorescein staining throughout the cornea, accumulating around the epithelial cells, indicating that these mice presented corneal epithelial erosion (Fig. 6A).

To confirm the increase in inflammatory cells within the corneas of wild-type, *HAS1*$^{-/-}$;*HAS3*$^{-/-}$, *HAS2*$^{\Delta CorEpi}$, and *TSG-6*$^{-/-}$ mice, the numbers of macrophages were counted within the corneas after whole-mount analysis 2 weeks after alkali burn. Wild-type mice presented ~15 F4/80^{+} cells within the stroma, *TSG-6*$^{-/-}$ mice ~40 F4/80^{+} cells, *HAS1*$^{-/-}$;*HAS3*$^{-/-}$ mice ~65 F4/80^{+} cells, and *HAS2*$^{\Delta CorEpi}$ mice ~75 F4/80^{+} cells (Fig. 6B). Therefore, *HAS1*$^{-/-}$;*HAS3*$^{-/-}$ and *HAS2*$^{\Delta CorEpi}$ mice presented a significant increase in the number of macrophages within the cornea when compared with wild-type mice (Fig. 6B). *TSG-6*$^{-/-}$ mice also presented a significant increase in the number of macrophages within the stroma when compared with wild-type mice (Fig. 6B).

Inflammation was also investigated by evaluating corneal haze using in vivo confocal microscopy. Two weeks after alkali burn, wild-type and *TSG-6*$^{-/-}$ mice presented a significant reduction of corneal haze, and inflammatory cells were barely evident within the stroma by in vivo confocal microscopy (Fig. 6D). On the other hand, *HAS1*$^{-/-}$;*HAS3*$^{-/-}$ and *HAS2*$^{\Delta CorEpi}$ mice presented a significant increase in both corneal haze and inflammatory cells within the stroma 2 weeks after alkali burn (Fig. 6D). Thus, wild-type and *TSG-6*$^{-/-}$ mice presented resolution of the inflammatory response by 2 weeks after alkali burn, whereas corneal inflammation persists in *HAS1*$^{-/-}$, *HAS3*$^{-/-}$, and *HAS2*$^{\Delta CorEpi}$ mice. The corneal epithelium was also evidenced by in vivo confocal microscopy (Fig. 6E). The goblet cells can also be seen in the corneal epithelium of *HAS2*$^{\Delta CorEpi}$ mice by in vivo confocal microscopy (Fig. 6E).

Corneal Scarring

To investigate whether the exacerbated inflammatory response leads to stromal scarring, SMAα staining was measured using whole-mount immunohistochemistry. Wild-type mice presented a mean of ~10 SMAα^{+} keratocytes per z-stack, *TSG-6*$^{-/-}$ mice ~20, *HAS1*$^{-/-}$;*HAS3*$^{-/-}$ mice ~45 and *HAS2*$^{\Delta CorEpi}$ mice ~65; however, there was significant variability within the groups (Fig. 6C). The *HAS1*$^{-/-}$;*HAS3*$^{-/-}$, *TSG-6*$^{-/-}$, and wild-type experimental groups all presented mice devoid of SMAα^{+} keratocytes; however, wild-type mice presented 62.5% of mice devoid of SMAα^{+} keratocytes, compared to 37.5% for *TSG-6*$^{-/-}$ mice and 25% for *HAS1*$^{-/-}$;*HAS3*$^{-/-}$ mice (Fig. 6C). However, in mice that did present scarring (SMAα^{+} keratocytes), there were significantly more SMAα^{+} keratocytes in *HAS1*$^{-/-}$;*HAS3*$^{-/-}$ and *HAS2*$^{\Delta CorEpi}$ mice. Wild-type mice that did present SMAα^{+} keratocytes had ~30 SMAα^{+} keratocytes per z-stack (37% of mice), whereas *TSG-6*$^{-/-}$ mice had ~40 (62.5% of mice), *HAS1*$^{-/-}$;*HAS3*$^{-/-}$ mice ~60 (75% of mice), and *HAS2*$^{\Delta CorEpi}$ mice ~65 (100% of mice). The mice that had SMAα^{+} keratocytes were also those that presented the most significant increase in inflammatory cells.

Hyaluronan Rich Limbal Stem Cell (LSC) Niche

Our data demonstrated that there was an intricate regulation of HAS expression in the corneal LSC niche after injury. To verify the expression profile of HA in the cornea, we localized HA in the corneas of wild-type, *HAS1*$^{-/-}$;*HAS3*$^{-/-}$, *HAS2*$^{\Delta CorEpi}$, and *TSG-6*$^{-/-}$ mice with the HA binding protein. Interestingly, wild-type corneal staining revealed that HA was specifically expressed in the limbal region, potentially comprising an HA rich limbal stem cell niche (Fig. 7). *HAS1*$^{-/-}$;*HAS3*$^{-/-}$ mice presented a loss of HA expression in the limbal region (Fig. 7). Thus we could infer that HAS1 and/or HAS3 are necessary for maintaining the limbal stem cell niche. *HAS2*$^{\Delta CorEpi}$ induced at P7 and P21 also presented a loss of HA in the LSC niche, and therefore we could infer that HAS2 is also necessary for maintaining HA in the LSC niche (Fig. 7). On the other hand, uninjured *TSG-6*$^{-/-}$ mice presented a slight increase in HA expression in the LSC niche, which spread into the peripheral stroma when compared with wild-type mice (Fig. 7). Thus, it is possible that TSG-6 is necessary for the structural organization of HA within the limbal region, and in its absence there is a compensatory mechanism that up-regulates HA expression. We also verified whether CD44, a well-known receptor for HA, is expressed by LSCs. All corneal epithelial cells, including LSCs, express CD44 (Supplementary Fig. S3). Changes in the distribution of CD44^{+} epithelial cells could be observed in *HAS1*$^{-/-}$;*HAS3*$^{-/-}$ and *HAS2*$^{\Delta CorEpi}$ mouse corneas (Supplementary Fig. S3). Both *HAS1*$^{-/-}$;*HAS3*$^{-/-}$ and *HAS2*$^{\Delta CorEpi}$ mice presented regions of densely stained CD44 epithelial cells, which presented an uneven cell shape.

Expression Profile of HA After Alkali Burn Wounding of Corneas From *HAS1*$^{-/-}$;*HAS3*$^{-/-}$, *HAS2*$^{\Delta CorEpi}$, and Wild-Type Mice

To verify the expression profile of HA after injury, HA was localized in the corneas of wild-type, *HAS1*$^{-/-}$;*HAS3*$^{-/-}$, *HAS2*$^{\Delta CorEpi}$, and *TSG-6*$^{-/-}$ mice 2 weeks after alkali burn. Interestingly, after injury *HAS1*$^{-/-}$;*HAS3*$^{-/-}$ mice presented a great increase in HA expression, which was no longer restricted to the limbal region, but spread throughout the entire corneal epithelium (Fig. 7B).

HAS2$^{\Delta CorEpi}$ mice also presented irregular epithelial cell sheets 2 weeks after alkali burn (dashed line, Fig. 7B), with some regions presenting epithelial cells growing into the stroma region (asterisks, Fig. 7B). Interestingly, *HAS2*$^{\Delta CorEpi}$ mice also presented K14^{-} cells within the cornea 2 weeks after alkali burn, which, as mentioned previously, were identified as goblet cells (Fig. 4). *TSG-6*$^{-/-}$ mice presented an increase in HA expression 2 weeks after alkali burn that was also no longer restricted to the limbal region, but present in the epithelium of the peripheral cornea (Fig. 7B).

Epithelial and Limbal Stem Cell Markers

Our findings suggest that corneal LSCs secrete an HA rich niche. To establish whether the HA within the limbal stem cell niche has a role in maintaining the limbal stem cells in their multipotent state, we analyzed the expression profile of LSCs (keratin 15, K15^{+} cells) and of differentiated epithelial cells (keratin 12, K12^{+} cells) in the corneas before and after alkali burn in the HA LSC niche and throughout the corneas of *HAS1*$^{-/-}$;*HAS3*$^{-/-}$, *HAS2*$^{\Delta CorEpi}$, *TSG-6*$^{-/-}$, and wild-type mice (Fig. 8). In the uninjured corneas, no obvious differences in K12^{+} cell expression were observed in *TSG-6*$^{-/-}$ mice when compared with wild-type mice. However, *HAS2*$^{\Delta CorEpi}$ induced at P7 presented K12^{+} cells in the limbus, and no K15^{+} cells, thus the loss of HA due to the ablation of HAS2 could lead to limbal stem cell deficiency in *HAS2*$^{\Delta CorEpi}$ induced at P7 or earlier (Fig. 8). On the other hand, *HAS1*$^{-/-}$;*HAS3*$^{-/-}$ and *HAS2*$^{\Delta CorEpi}$ mice induced at P21 presented an increase in

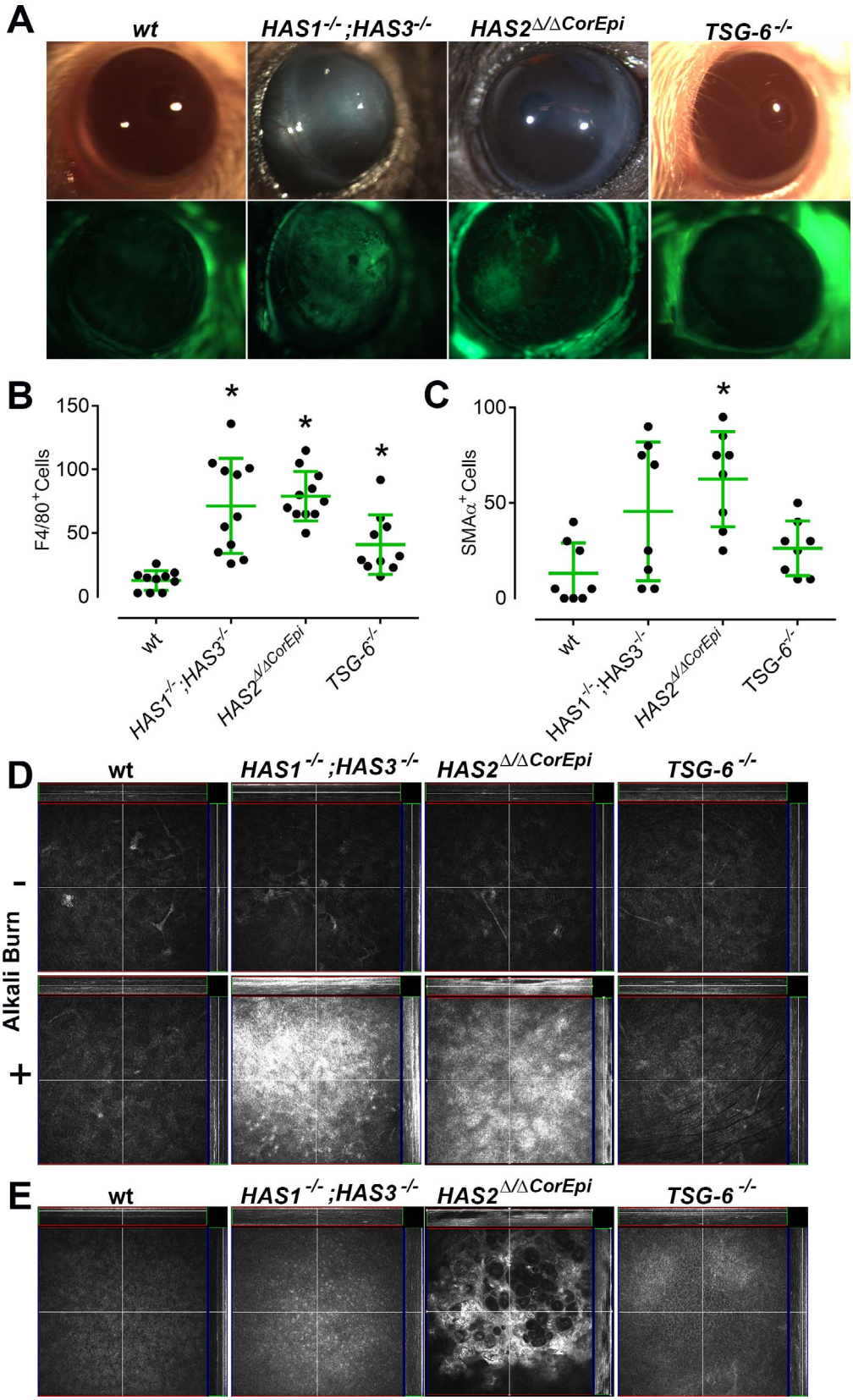

Figure 6. Analysis of corneal integrity and inflammation after injury. *HAS1*$^{-/-}$;*HAS3*$^{-/-}$, *HAS2*$^{\Delta/\Delta CorEpi}$, *TSG-6*$^{-/-}$, and wild-type mice were subjected to alkali burn and 2 weeks later analyzed using a stereomicroscope. Images were captured using a white light (**A**, *top*). To assess corneal integrity, fluorescein was placed on the ocular surface, and subsequently the eye was washed and the cornea imaged under a fluorescent stereomicroscope (A, *bottom*). Whole-mount staining for F4/80^{+} cells and SMAα was done on corneas of *HAS1*$^{-/-}$;*HAS3*$^{-/-}$, *HAS2*$^{\Delta/\Delta CorEpi}$, *TSG-6*$^{-/-}$, and wild-type mice 2 weeks after alkali burn. The numbers of F4/80^{+} cells and SMAα^{+} cells were counted in a blinded manner (**B, C**, respectively). Corneal haze and inflammation in *HAS1*$^{-/-}$;*HAS3*$^{-/-}$, *HAS2*$^{\Delta/\Delta CorEpi}$, *TSG-6*$^{-/-}$, and wild-type mice were assessed by in vivo confocal microscopy (**D**). The corneal epithelial morphology 2 weeks after alkali burn was assessed by in vivo confocal microscopy (**E**).

Investigative Ophthalmology & Visual Science

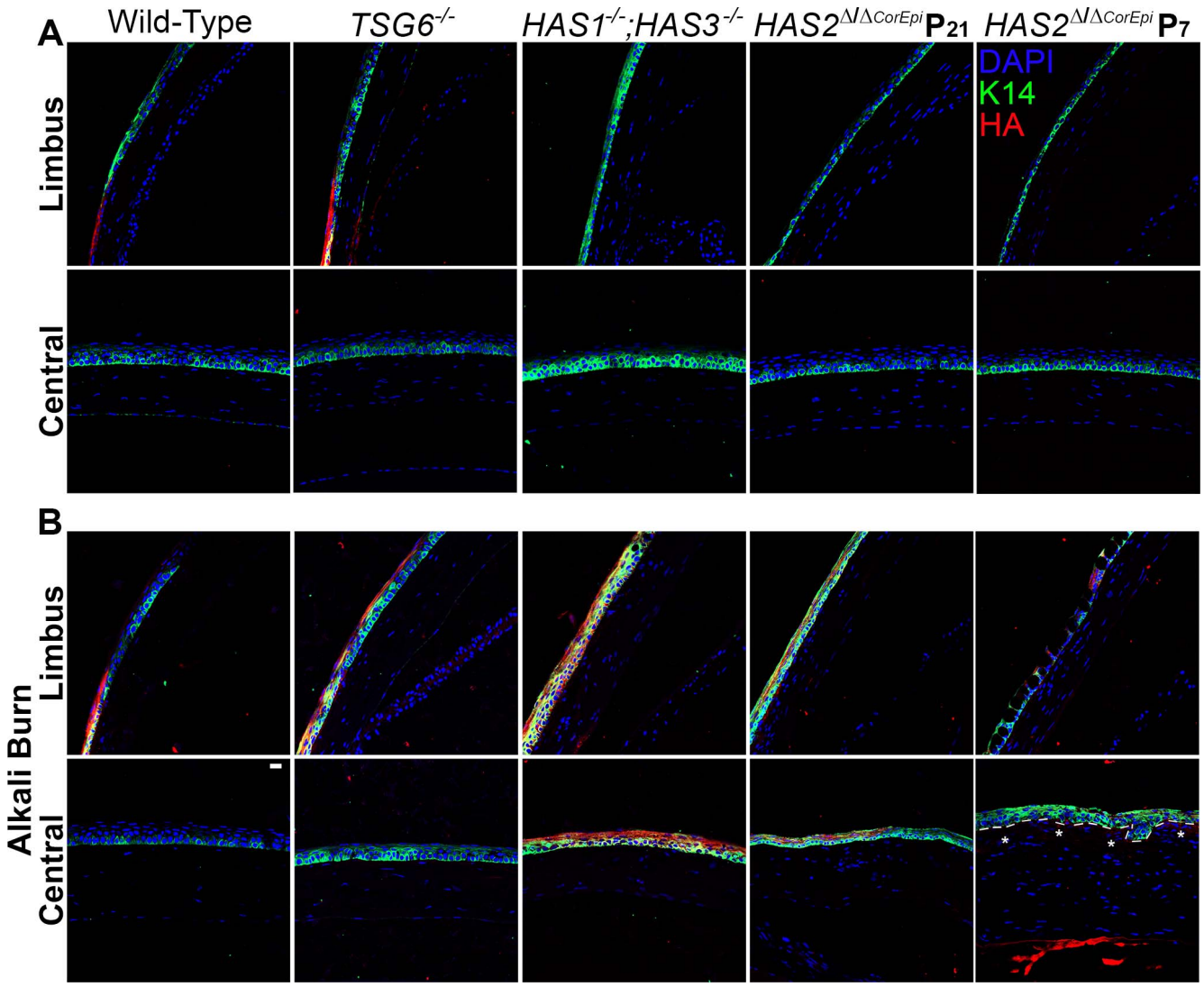

Figure 7. Expression profiles of HA and K14 in the corneas of *HAS1*$^{-/-}$;*HAS3*$^{-/-}$, *HAS2*$^{\Delta/\Delta CorEpi}$, *TSG-6*$^{-/-}$, and wild-type mice. HA (*red*) and K14 (*green*) were stained in uninjured (**A**) and alkali burnt (**B**) corneas of *HAS1*$^{-/-}$;*HAS3*$^{-/-}$, *HAS2*$^{\Delta/\Delta CorEpi}$ (induced at P21 and P7), *TSG-6*$^{-/-}$, and wild-type mice and images captured of the limbal region (Limbus) and central cornea (Central). The *TSG-6*$^{-/-}$ and wild-type mice show HA staining in the corneal limbus, whereas *HAS1*$^{-/-}$;*HAS3*$^{-/-}$ and *HAS2*$^{\Delta/\Delta CorEpi}$ (induced at P21 and P7) mice lack HA staining in the limbus. Two weeks after alkali burn, *TSG-6*$^{-/-}$ mice present an increase in HA expression into the peripheral cornea, *HAS1*$^{-/-}$;*HAS3*$^{-/-}$ and *HAS2*$^{\Delta/\Delta CorEpi}$ (induced at P21 and P7) mice express HA throughout the entire cornea, whereas wild-type mice present no changes in HA expression after injury. The *dashed line* (*lower right* image) shows the division between epithelial cells and the stroma and the asterisks mark where epithelial cells are growing into the stroma. *Scale bar*: 20 μm.

K15^{+} cells into the peripheral cornea, which was more significant in the *HAS1*$^{-/-}$, *HAS3*$^{-/-}$ mice (Fig. 8). Interestingly, after alkali burn, *HAS1*$^{-/-}$;*HAS3*$^{-/-}$ and *HAS2*$^{\Delta CorEpi}$ mice presented a loss of K12^{+} cells in the central and peripheral corneas. These mice also presented an increase in K15^{+} cells, which became present throughout the cornea, coinciding with the increase in HA expression (Fig. 8). Therefore, *HAS1*$^{-/-}$;*HAS3*$^{-/-}$ and *HAS2*$^{\Delta CorEpi}$ mice presented expression of the limbal stem cell niche (HA) throughout the cornea, which led to the presence of LSCs (K15^{+} cells) throughout the entire corneal epithelium. The presence of K12^{-}/K15^{-} cells in the corneas of *HAS2*$^{\Delta CorEpi}$ mice after alkali burn could be noted, which were identified as goblet cells (Fig. 4). *TSG-6*$^{-/-}$ mice present K15^{+} cells in the peripheral cornea, which also coincided with the extended HA expression in the peripheral cornea (Fig. 8).

Ex Vivo Debridement Wounding of Corneas From *HAS1*$^{-/-}$;*HAS3*$^{-/-}$, *HAS2*$^{\Delta CorEpi}$, and Wild-Type Mice

To evaluate the role of HA on corneal healing without the influence of inflammatory cell infiltration, we analyzed ex vivo debridement wounds. For such, the corneas were injured, eyeballs enucleated, and the corneas allowed to heal for 24 hours in explant culture conditions. The size of the wound area was measured as the fluorescein positive area at 0, 6, 12, and 24 hours after injury. Six hours after the debridement wound, *HAS1*$^{-/-}$;*HAS 3*$^{-/-}$ mice displayed a slight increase in the wounded area when compared with 0 hours due to a receding wound edge (Fig. 9A). This could be due to the eventual cell death or desquamation of cells that were damaged during the injury or in close proximity to the wounded area. The wounded area did not significantly change in *HAS2*$^{\Delta CorEpi}$ mice by 6 hours after the debridement wound.

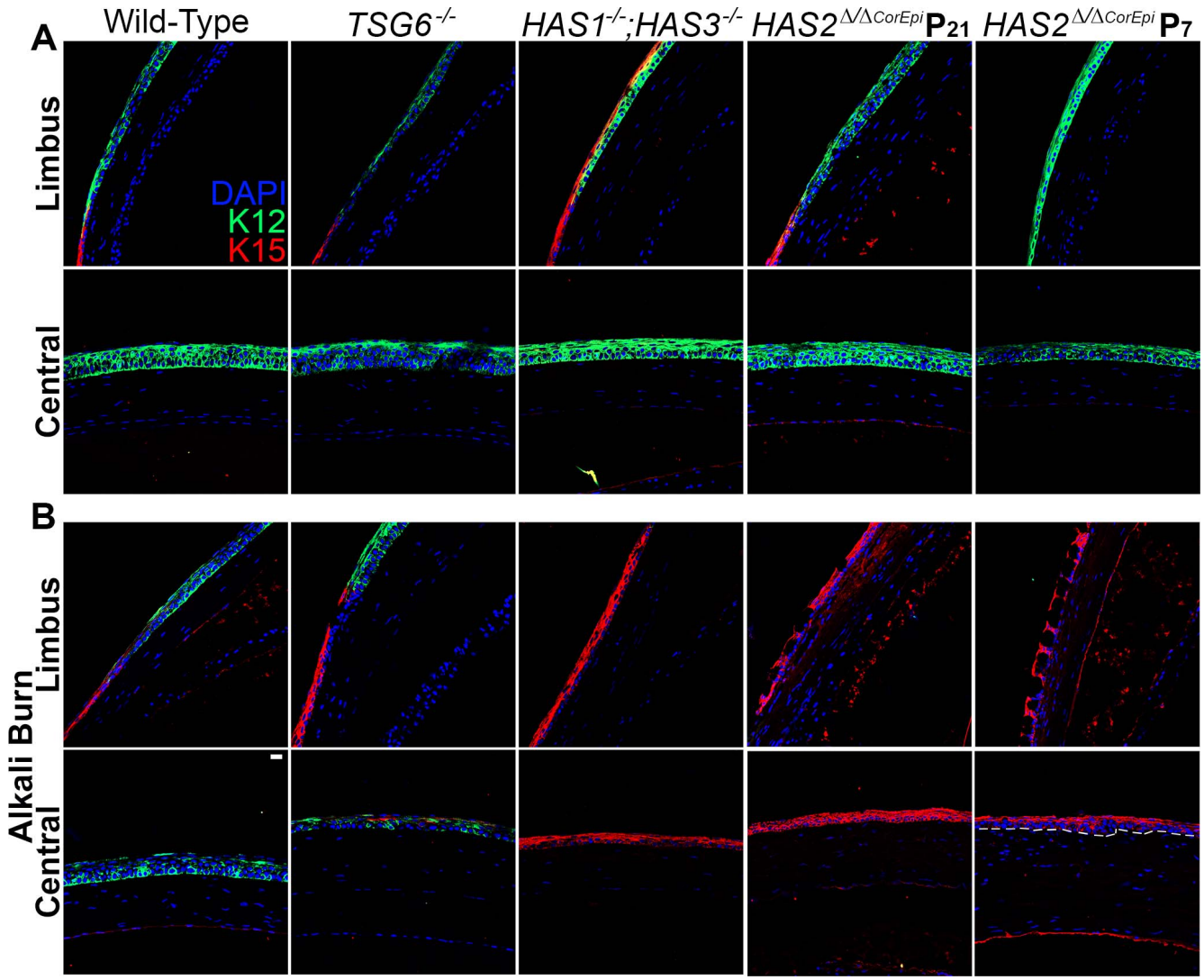

Figure 8. Expression profiles of K12 and K15 cells in the cornea of *HAS1*$^{-/-}$;*HAS3*$^{-/-}$, *HAS2*$^{\Delta/\Delta CorEpi}$, *TSG-6*$^{-/-}$, and wild-type mice. K12 (*green*) and K15 (*red*) cells were stained in uninjured (**A**) and alkali burnt (**B**) corneas of *HAS1*$^{-/-}$;*HAS3*$^{-/-}$, *HAS2*$^{\Delta/\Delta CorEpi}$ (induced at P21 and P7), *TSG-6*$^{-/-}$, and wild-type mice and images captured of the limbal region (Limbus) and central cornea (Central). *HAS2*$^{\Delta/\Delta CorEpi}$ (induced at P21), *TSG-6*$^{-/-}$, and wild-type mice present K15^{+} cells exclusively in the corneal limbus in uninjured corneas. *HAS1*$^{-/-}$;*HAS3*$^{-/-}$ mice present an increase in K15^{+} cells into the peripheral cornea, and in contrast *HAS2*$^{\Delta/\Delta CorEpi}$ (induced at P7) lack K15^{+} cells in the corneal limbus. Two weeks after alkali burn, *HAS1*$^{-/-}$;*HAS3*$^{-/-}$ and *HAS2*$^{\Delta/\Delta CorEpi}$ (induced at P21 and P7) mice present K15^{+} cells throughout the cornea and in turn lack K12^{+} cells. The *dashed line* (*lower right* image) shows the division between epithelial cells and the stroma. *Scale bar*: 20 μm.

On the other hand, wild-type mice presented a 15% decrease in the wounded area 6 hours after the debridement wound (Fig. 9A). Twelve hours after the debridement wound, all wild-type mice displayed a significant reduction in the wounded area when compared with both 0 and 6 hours, with a mean wounded area of 68% when compared with 0 hours (Fig. 9A). In contrast, for *HAS1*$^{-/-}$;*HAS3*$^{-/-}$ mice the wound edges receded further at 12 hours after injury, and 11 of the 14 *HAS1*$^{-/-}$;*HAS3*$^{-/-}$ mice presented increases in wounded area, with a mean wounded area of 108% when compared with 0 hours (Fig. 9A). *HAS2*$^{\Delta CorEpi}$ mice presented no changes in the wounded area 12 hours after debridement wound. Twenty-four hours after the debridement wound, all mice presented significant reductions in the wounded area; however, the wounded areas in *HAS1*$^{-/-}$;*HAS3*$^{-/-}$ and *HAS2*$^{\Delta CorEpi}$ mice were significantly larger than in wild-type mice, with wounded areas at ~82, ~78, and ~17%, respectively (Fig. 9A). Therefore, *HAS1*$^{-/-}$;*HAS3*$^{-/-}$ and *HAS2*$^{\Delta CorEpi}$ mice clearly displayed delayed wound healing when compared to wild-type mice.

The eyeballs were processed for histology 24 hours after the debridement wound. *HAS1*$^{-/-}$;*HAS3*$^{-/-}$ mice presented an accumulation of epithelial cells at the wound edge, which could be due to an inability of the epithelial cells to migrate along the basement membrane (Fig. 9B). This would be consistent with the findings that *HAS1*$^{-/-}$;*HAS3*$^{-/-}$ mice present reduced adhesion complexes between the epithelial cells and the basement membrane. On the other hand, *HAS2*$^{\Delta CorEpi}$ mice presented a reduction of corneal epithelial cell layers, indicating that these mice could present reduced cell proliferation, which would culminate in the delayed wound healing (Fig. 9B). Neither the wild-type, *HAS1*$^{-/-}$;*HAS3*$^{-/-}$, nor *HAS2*$^{\Delta CorEpi}$ mice presented HA staining at the wound edge (Fig. 9C). However, *HAS1*$^{-/-}$;*HAS3*$^{-/-}$ presented an increase in K15^{+} cells in the corneal limbus, whereas in contrast *HAS2*$^{\Delta CorEpi}$ mice presented a decrease in the number

Investigative Ophthalmology & Visual Science

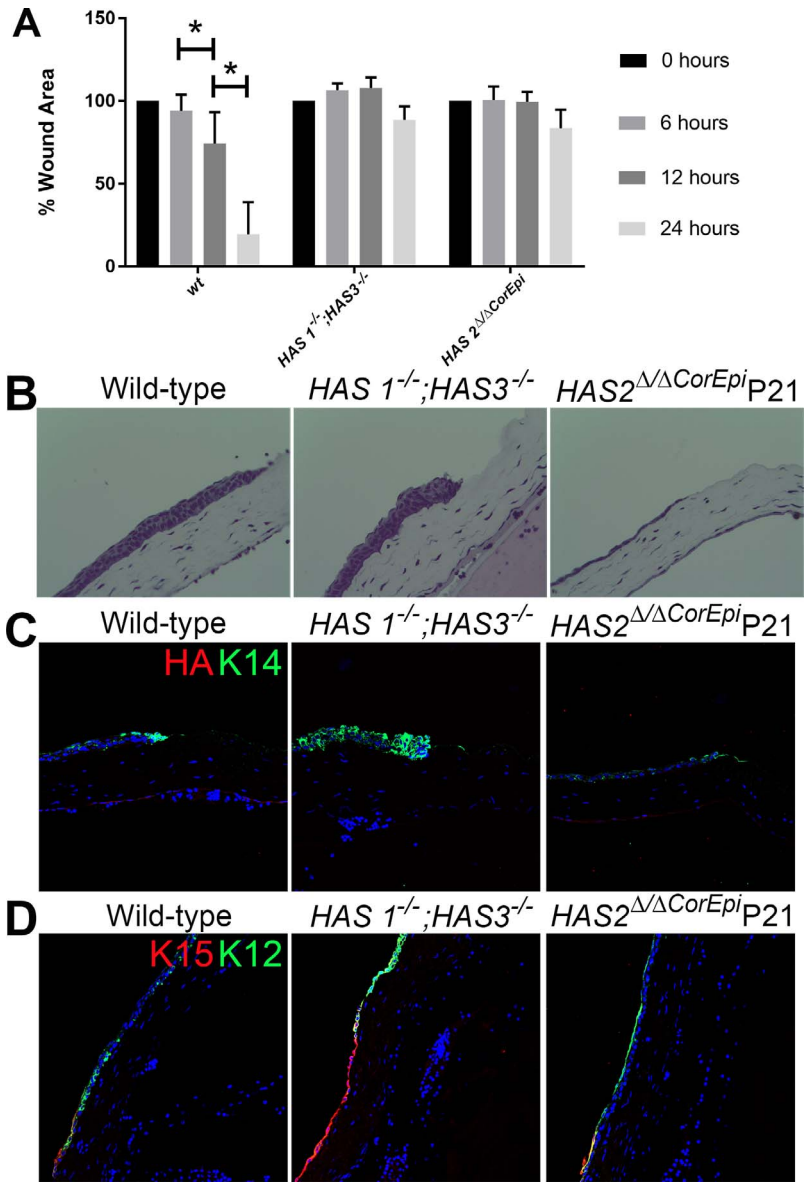

Figure 9. *HAS1*$^{-/-}$*;HAS3*$^{-/-}$ and *HAS2*$^{\Delta/\Delta CorEpi}$ mice show delayed wound healing using an ex vivo debridement wound model. *HAS1*$^{-/-}$*;HAS3*$^{-/-}$, *HAS2*$^{\Delta/\Delta CorEpi}$ (induced at P21), and wild-type mice were euthanized, debridement wounds were made on the central cornea, and eyeballs were removed and placed in culture. The rate of wound healing was assessed at 6, 12, and 24 hours by placing a drop of fluorescein on the eyeball and washing and capturing images using a fluorescence stereomicroscope. The wound area was measured and plotted in a graph as the percentage of wound area remaining (**A**). $^*P \leq 0.05$ compared to 0 hours. *HAS1*$^{-/-}$*;HAS3*$^{-/-}$ and *HAS2*$^{\Delta/\Delta CorEpi}$ mice had delayed wound healing when compared with wild-type mice. The eyeballs were fixed 24 hours after injury for histological analysis. (**B**) H&E staining showed that *HAS1*$^{-/-}$*;HAS3*$^{-/-}$ mice accumulate epithelial cells at the wound edge, whereas *HAS2*$^{\Delta/\Delta CorEpi}$ have a reduced number of epithelial cell layers. Tissue sections were also stained for HA (*red*) and K14 (*green*; **C**), K15 (*red*), and K12 (*green*; **D**). Nuclei were counterstained with DAPI (*blue*).

of K15$^+$ cells in the corneal limbus when compared with wild-type mice (Fig. 9D).

Discussion

Hyaluronan is a ubiquitous component of the extracellular matrix that is enriched during the early stages of development and disease, and recent studies have demonstrated that HA matrices have an important role in the stem cell niche. We have demonstrated that human umbilical cord mesenchymal stem cells secrete a specific HA/HC/TSG-6/PTX3/versican glycocalyx that enables these cells to survive xenograft rejection increasing their engraftment success.[42] Following our work, TSG-6, HA and exogenous IαI were shown to increase embryonic MSC engraftment into skeletal muscle and favor differentiation into muscle cells.[65] The authors speculated that TSG-6, HA, and IαI were assembling into a glycocalyx that favored MSC engraftment.[65] This group went on to show that TSG-6, HA, and IαI assemble to form a microenvironment necessary for successful MSC engraftment and that enables the subsequent differentiation of MSCs.[65] We hereby show that HA is also a vital component of the corneal LSC niche.

The size of the HA chains has an important role during matrix assembly, composition, and function. Studies have shown that primarily two forms of HA exist: HMWHA of approximately 2,000 kDa and LMWHA of approximately 200 kDa.[46,66–68] HA chains are synthesized by HAS1, HAS2, or

HAS3; however, a basic understanding on how HAS enzymes regulate the length of the growing HA chain during the biosynthetic process, which greatly affects its physiological function, remains unknown. It has also been speculated that HAS1 and HAS3 produce primarily HMWHA, whereas HAS2 produces primarily LMWHA.[69,70] Interestingly, naked mole rat (*Heterocephalus glaber*) fibroblasts have been shown to secrete extremely high-molecular-weight hyaluronan, more than five times larger than that found in other mammals, including humans. This extremely high-molecular-weight hyaluronan contributes to the exceptionally high longevity and unusual resistance to cancer displayed by naked mole rats.[71–76] The different HAS enzymes present a specific special-temporal distribution throughout development.[77] Interestingly, our work shows that all three HAS enzymes are expressed in the LSC niche and that all three are required to produce a transient HA matrix that supports cornea regeneration after injury.

To elucidate the role of the different HAS enzymes in maintaining the HA matrix in the LSC niche, we used knockout mice for the different HAS enzymes. HAS2 is the most widely distributed HAS in tissues, thus the *HAS2 null* mouse is embryonic lethal. Therefore, we generated a conditional knock-out mouse model to remove *HAS2* from $K14^+$ cells, which would include corneal LSCs and corneal epithelial cells. Curiously, both $HAS1^{-/-};HAS3^{-/-}$ mice and $HAS2^{\Delta CorEpi}$ mice presented a loss of HA in the LSC niche. The loss of HA in the LSC niche did not lead to corneal dysgenesis in any of the uninjured $HAS1^{-/-};HAS3^{-/-}$ or $HAS2^{\Delta CorEpi}$ mice, indicating that epithelial cell proliferation is sufficient to maintain a stratified epithelium in unchallenged corneas. The corneal epithelium is a continuously regenerating tissue maintained by basal cells that undergo mitosis, and dividing cells move upward to replenish wing cells.[78,79] As the new cells move upward, superficial squamous cells slough off. Corneal LSCs are highly proliferative undifferentiated cells that provide an unlimited supply of proliferating cells to replenish corneal epithelial cells after injury.[79,80] Therefore, our results support the hypothesis that unchallenged corneas are maintained primarily by basal epithelial cells. Previous studies have reported that the vertical turnover of the corneal stratified epithelium in mammals ranges from 7 to 14 days and suggest that limbal stem cells are necessary for long-term renewal of the epithelium.[7,81] However, the Tseng group have elegantly shown that the corneal epithelium can self-sustain in the absence of the corneal limbus up until the point that the epithelium is perturbed.[82] Majo et al.[83] have also shown that limbal stem cells solely migrate from the limbus onto the cornea after injury. This study also demonstrated that cauterization of the entire limbal circumference, which would destroy both limbal stem cells and the limbal stem cell niche, does not lead to impaired vision.[83] Our data further reinforce the notion that limbal stem cells are not required for maintaining the corneal epithelium during homeostasis. $HAS1^{-/-};HAS3^{-/-}$ and $HAS2^{\Delta CorEpi}$ mice showed impaired wound healing after both ex vivo debridement wound and alkali burn. The ex vivo debridement wound model was used to study the effect of HA in the LSC niche on wound healing without the influence of infiltrating inflammatory cells. The alkali burn model was used to evaluate the role of HA in the LSC niche on cornea regeneration and inflammation. Our alkali burn model spares the LSCs, and wild-type mouse corneas were fully healed at 2 weeks after injury and no longer presented signs of inflammatory response. On the other hand, $HAS1^{-/-};HAS3^{-/-}$ mice and $HAS2^{\Delta CorEpi}$ mice showed increased inflammatory response and failure to form a stratified epithelium after injury.

We also investigated whether the HA in the LSC niche could have a role in regulating LSC specification. For such, we stained for LSCs ($K15^+$ cells) and differentiated corneal epithelial cells ($K12^+$ cells) in $HAS1^{-/-};HAS3^{-/-}$ and $HAS2^{\Delta CorEpi}$ mice. Interestingly, $HAS2^{\Delta CorEpi}$ mice induced at P7 presented a loss of LSCs in the corneal limbus, indicating that the loss of HAS2 leads to LSCD. Moreover, $HAS2^{\Delta CorEpi}$ mice presented primarily goblet cells in the peripheral cornea and sparse goblet cells in the central cornea after alkali burn. A hallmark of LSCD is conjunctivalization of the cornea, which is the invasion of conjunctival surface cells (goblet cells) onto the corneal surface.[3,26] Therefore, the presence of goblet cells in the corneal epithelium after injury further supports the notion that the loss of HAS2 leads to LSCD. Taken together, our results indicate that $HAS2^{\Delta CorEpi}$ mice could be a useful model for studying LSCD. Curiously, after injury, both $HAS1^{-/-};HAS3^{-/-}$ and $HAS2^{\Delta CorEpi}$ mice presented an increase in HA expression, which, after alkali burn, is present throughout the cornea. Therefore, $HAS1^{-/-};HAS3^{-/-}$ mice up-regulate HAS2 as a compensatory mechanism after injury, whereas $HAS2^{\Delta CorEpi}$ mice up-regulate HAS1 and/or HAS3 expression after injury. The change in HA distribution in the cornea from being located solely in the corneal limbus to being expressed throughout the corneal epithelium in turn alters the distribution of LSCs. Interestingly, the change in HA distribution leads to the presence of LSCs throughout the corneal epithelium and the absence of differentiated corneal epithelial cells. These data indicate that the HA microenvironment maintains the LSC phenotype. Thus, as LSCs migrate out of the LSC niche, the lack of an HA environment could trigger their differentiation into corneal epithelial cells. Curiously, $HAS2^{\Delta CorEpi}$ mice induced at P7 lacked both HA and LSCs ($K15^+$ cells) in the corneal limbus and instead presented corneal epithelial cells ($K12^+$ cells); however, after injury these mice were able to switch from solely $K12^+$ cells to $K15^+$ cells. How mice lacking LSCs were able to generate de novo LSCs remains to be determined. Previous studies have demonstrated that corneal epithelial cells have high regenerative and migratory potential.[83,84] Moreover, Majo et al.[83] were also able to show that corneal epithelial cells could assume either a conjunctival or epithelial cell phenotype depending on the site of transplantation; however, these findings have been met with some controversy. Our data show that the $K12^+$ to $K15^+$ cell switch coincides with the up-regulation of HA, further indicating that HA could regulate LSC and corneal epithelial specification. Therefore, the up-regulation of HA synthesis within the corneal limbus could provide a viable therapeutic approach for treating LSCD. Whether the ultrastructure and composition of the HA matrix and length of the HA chains present throughout the cornea in $HAS1^{-/-};HAS3^{-/-}$ and $HAS2^{\Delta CorEpi}$ mice after injury are similar to the HA found in the healthy LSC niche remains to be elucidated. $TSG\text{-}6^{-/-}$ mice showed altered HA expression in the LSC niche and increased inflammation after alkali burn. In the $TSG\text{-}6^{-/-}$ mice the absence of TSG-6 could potentially lead to a less compact/stable HA matrix, which could affect the migration of LSCs and inflammatory cells. Therefore, our data indicate that potentially a specialized HC-HA/TSG-6 matrix could be present in the corneal LSC niche; however, further research is necessary to fully characterize the composition of this matrix. Amniotic membrane based therapies for treating LSCD have been studied for many years.[30,31,56,85,86] The Tseng group have determined that a HC-HA/PTX3 complex is the pharmacologically active component of the amniotic membrane commonly used for treating ocular surface disorders, including LSCD.[30] Substantial studies have demonstrated that HC-HA/PTX3 complexes attain powerful anti-inflammatory properties, and this complex was hypothesized to improve the outcome of LSCD patients by suppressing the inflamma-

tory response. Our data indicate that the therapeutic properties of the amniotic membrane could go beyond simply suppressing inflammation. The HC-HA/TSG-6 complex released by the amniotic membrane could provide support to LSCs forming a transient LSC niche for any residual LSCs.

Corneal injury that leads to substantial damage to LSCs or the LSC niche decreases the number of LSCs and thereby reduces the ability of these cells to resurface the corneal epithelium. A significant loss of LSCs or the LSC niche leads to LSCD. LSCD patients present recurring erosions, corneal inflammation, severe pain, and eventual conjunctivalization of the cornea.[32] TSG-6 and HA matrices have a well-established role in inflammation; assembly of the HC-HA/TSG-6 matrix has been shown to be immunosuppressive, protecting tissues from the detrimental effects of inflammation.[42,85,86] Therefore, damage to the LSC niche and consequently the loss of this HA specific environment in the cornea/conjunctiva zone could be in part responsible for the increase in inflammatory cell infiltration in LSCD patients. Moreover, evidence suggests that the limbus may contain essential cues to limit the migration of conjunctival cells into the cornea, thereby precluding conjunctivalization in a normal cornea. Our data show that $HAS2^{\Delta CorEpi}$ mice present goblet cell invasion into the peripheral and central cornea. LSCD patients eventually present conjunctivalization, which in turn leads to severe vision loss. Because LSCD involves the loss of both LSCs and the LSC niche, we could hypothesize that loss of the HA-specific LSC niche could be in part responsible for the migration of conjunctival cells onto the cornea in LSCD patients. Currently, the largest hurdle in developing limbal stem cell transplantation is the efficient expansion of donor limbal stem cells ex vivo prior to transplantation. Our work clearly demonstrates that HA is essential for maintaining the LSC phenotype.

This study identified a HA specific matrix present in the cornea exclusively in the LSC niche. The disruption of this HA matrix within the LSC niche leads to increased inflammatory response after injury and altered LSC and corneal epithelial cell specification. Follow-up work will aim to characterize the precise structural composition of this HA matrix and identify the precise length of the HA chains present in the LSC niche.

Acknowledgments

The authors dedicate this work to the remembrance of Mark Lauer. The authors thank Kazadi Nadine Mutoji for her invaluable technical assistance, Naoki Itano for kindly providing HAS1 *null* mice, and Winston Kao for kindly providing the K14 rtta and tet-O-cre mice. They also thank the Department of Ophthalmology from the University of Cincinnati for their support during the transition to Houston.

Presented in part at the annual meeting of the Association for Research in Vision and Ophthalmology, Baltimore, Maryland, United States, May 2017.

Supported by start-up funds from the University of Houston, The Mizutani Foundation, and the National Institutes of Health/National Eye Institute Core Grant P30 EY07551.

Disclosure: **T.F. Gesteira**, None; **M. Sun**, None; **Y.M. Coulson-Thomas**, None; **Y. Yamaguchi**, None; **L.-K. Yeh**, None; **V. Hascall**, None; **V.J. Coulson-Thomas**, None

References

1. Shortt AJ, Secker GA, Munro PM, Khaw PT, Tuft SJ, Daniels JT. Characterization of the limbal epithelial stem cell niche: novel imaging techniques permit in vivo observation and targeted biopsy of limbal epithelial stem cells. *Stem Cell*. 2007;25:1402–1409.
2. Dziasko MA, Armer HE, Levis HJ, Shortt AJ, Tuft S, Daniels JT. Localisation of epithelial cells capable of holoclone formation in vitro and direct interaction with stromal cells in the native human limbal crypt. *PLoS One*. 2014;9:e94283.
3. Dua HS, Azuara-Blanco A. Limbal stem cells of the corneal epithelium. *Surv Ophthalmol*. 2000;44:415–425.
4. Ebrahimi M, Taghi-Abadi E, Baharvand H. Limbal stem cells in review. *J Ophthalmic Vis Res*. 2009;4:40–58.
5. Potten CS, Loeffler M. Stem cells: attributes, cycles, spirals, pitfalls and uncertainties. Lessons for and from the crypt. *Development*. 1990;110:1001–1020.
6. Lavker RM, Wei ZG, Sun TT. Phorbol ester preferentially stimulates mouse fornical conjunctival and limbal epithelial cells to proliferate in vivo. *Invest Ophthalmol Vis Sci*. 1998;39:301–307.
7. Cotsarelis G, Cheng SZ, Dong G, Sun TT, Lavker RM. Existence of slow-cycling limbal epithelial basal cells that can be preferentially stimulated to proliferate: implications on epithelial stem cells. *Cell*. 1989;57:201–209.
8. Zhang Y, Sun H, Liu Y, et al. The limbal epithelial progenitors in the limbal niche environment. *Int J Med Sci*. 2016;13:835–840.
9. Haagdorens M, Van Acker SI, Van Gerwen V, et al. Limbal stem cell deficiency: current treatment options and emerging therapies. *Stem Cell Int*. 2016;2016:9798374.
10. Lavker RM, Sun TT. Epidermal stem cells: properties, markers, and location. *Proc Natl Acad Sci U S A*. 2000;97:13473–13475.
11. Potten CS, Booth C. Keratinocyte stem cells: a commentary. *J Invest Dermatol*. 2002;119:888–899.
12. Kenyon KR, Tseng SC. Limbal autograft transplantation for ocular surface disorders. *Ophthalmology*. 1989;96:709–722; discussion 722–703.
13. Tseng SC. Concept and application of limbal stem cells. *Eye (Lond)*. 1989;3(Pt 2):141–157.
14. Tseng SC. Significant impact of limbal epithelial stem cells. *Indian J Ophthalmol*. 2000;48:79–81.
15. Tan DT, Ficker LA, Buckley RJ. Limbal transplantation. *Ophthalmology*. 1996;103:29–36.
16. Pellegrini G, Traverso CE, Franzi AT, Zingirian M, Cancedda R, De Luca M. Long-term restoration of damaged corneal surfaces with autologous cultivated corneal epithelium. *Lancet*. 1997;349:990–993.
17. Lagali N, Eden U, Utheim TP, et al. In vivo morphology of the limbal palisades of vogt correlates with progressive stem cell deficiency in aniridia-related keratopathy. *Invest Ophthalmol Vis Sci*. 2013;54:5333–5342.
18. Le Q, Yang Y, Deng SX, Xu J. Correlation between the existence of the palisades of Vogt and limbal epithelial thickness in limbal stem cell deficiency. *Clin Exp Ophthalmol*. 2017;45:224–231.
19. Ksander BR, Kolovou PE, Wilson BJ, et al. ABCB5 is a limbal stem cell gene required for corneal development and repair. *Nature*. 2014;511:353–357.
20. Moll R, Franke WW, Schiller DL, Geiger B, Krepler R. The catalog of human cytokeratins: patterns of expression in normal epithelia, tumors and cultured cells. *Cell*. 1982;31:11–24.
21. Tseng SC, Jarvinen MJ, Nelson WG, Huang JW, Woodcock-Mitchell J, Sun TT. Correlation of specific keratins with different types of epithelial differentiation: monoclonal antibody studies. *Cell*. 1982;30:361–372.
22. Sun T-T, Eichner R, Schermer A, Cooper D, Nelson W, Weiss R. *Classification, Expression, and Possible Mechanisms of Evolution of Mammalian Epithelial Keratins: A Unifying Model*. New York: Cold Spring Harbor; 1984.

23. Schermer A, Galvin S, Sun TT. Differentiation-related expression of a major 64K corneal keratin in vivo and in culture suggests limbal location of corneal epithelial stem cells. *J Cell Biol*. 1986;103:49–62.
24. Dua HS, Saini JS, Azuara-Blanco A, Gupta P. Limbal stem cell deficiency: concept, aetiology, clinical presentation, diagnosis and management. *Indian J Ophthalmol*. 2000;48:83–92.
25. Ahmad S. Concise review: limbal stem cell deficiency, dysfunction, and distress. *Stem Cells Trans Med*. 2012;1: 110–115.
26. Dua HS, Azuara-Blanco A. Autologous limbal transplantation in patients with unilateral corneal stem cell deficiency. *Br J Ophthalmol*. 2000;84:273–278.
27. Burman S, Sangwan V. Cultivated limbal stem cell transplantation for ocular surface reconstruction. *Clin Ophthalmol*. 2008;2:489–502.
28. Bakhtiari P, Djalilian A. Update on limbal stem cell transplantation. *Middle East Afr J Ophthalmol*. 2010;17:9–14.
29. De Luca M, Pellegrini G, Green H. Regeneration of squamous epithelia from stem cells of cultured grafts. *Regen Med*. 2006; 1:45–57.
30. Tseng SC. HC-HA/PTX3 purified from amniotic membrane as novel regenerative matrix: insight into relationship between inflammation and regeneration. *Invest Ophthalmol Vis Sci*. 2016;57:ORSFh1–ORSFh8.
31. Liu J, Sheha H, Fu Y, Liang L, Tseng SC. Update on amniotic membrane transplantation. *Exp Rev Ophthalmol*. 2010;5: 645–661.
32. Sejpal K, Bakhtiari P, Deng SX. Presentation, diagnosis and management of limbal stem cell deficiency. *Middle East Afr J Ophthalmol*. 2013;20:5–10.
33. Hascall V, Esko JD. Hyaluronan. In: Varki A, Cummings RD, Esko JD, Freeze HH, Stanley P, Bertozzi CR, eds. *Essentials of Glycobiology*. New York: Cold Spring Harbor; 2009:219–228.
34. Hascall VC. Hyaluronan, a common thread. *Glycoconj J*. 2000; 17:607–616.
35. McDonald J, Hascall VC. Hyaluronan minireview series. *J Biol Chem*. 2002;277:4575–4579.
36. Lee JY, Spicer AP. Hyaluronan: a multifunctional, megaDalton, stealth molecule. *Curr Opin Cell Biol*. 2000;12:581–586.
37. Bollyky PL, Falk BA, Wu RP, Buckner JH, Wight TN, Nepom GT. Intact extracellular matrix and the maintenance of immune tolerance: high molecular weight hyaluronan promotes persistence of induced CD4+CD25+ regulatory T cells. *J Leukocyte Biol*. 2009;86:567–572.
38. Karbownik MS, Nowak JZ. Hyaluronan: towards novel anticancer therapeutics. *Pharmacol Rep*. 2013;65:1056–1074.
39. Ruppert SM, Hawn TR, Arrigoni A, Wight TN, Bollyky PL. Tissue integrity signals communicated by high-molecular weight hyaluronan and the resolution of inflammation. *Immunol Res*. 2014;58:186–192.
40. Singleton PA. Hyaluronan regulation of endothelial barrier function in cancer. *Adv Cancer Res*. 2014;123:191–209.
41. Stern R. Hyaluronidases in cancer biology. *Sem Cancer Biol*. 2008;18:275–280.
42. Coulson-Thomas VJ, Gesteira TF, Hascall V, Kao W. Umbilical cord mesenchymal stem cells suppress host rejection: the role of the glycocalyx. *J Biol Chem*. 2014;289:23465–23481.
43. Coulson-Thomas VJ, Lauer ME, Soleman S, et al. Tumor necrosis factor-stimulated gene-6 (TSG-6) is constitutively expressed in adult central nervous system (CNS) and associated with astrocyte-mediated glial scar formation following spinal cord injury. *The J Biol Chem*. 2016;291: 19939–19952.
44. Lee RH, Pulin AA, Seo MJ, et al. Intravenous hMSCs improve myocardial infarction in mice because cells embolized in lung are activated to secrete the anti-inflammatory protein TSG-6. *Cell Stem Cell*. 2009;5:54–63.
45. Wisniewski HG, Vilcek J. TSG-6: an IL-1/TNF-inducible protein with anti-inflammatory activity. *Cytokine Growth Factor Rev*. 1997;8:143–156.
46. Salustri A, Yanagishita M, Hascall VC. Synthesis and accumulation of hyaluronic acid and proteoglycans in the mouse cumulus cell-oocyte complex during follicle-stimulating hormone-induced mucification. *J Biol Chem*. 1989;264:13840–13847.
47. Yanagishita M, Salustri A, Hascall VC. Specific activity of radiolabeled hexosamines in metabolic labeling experiments. *Methods Enzymol*. 1989;179:435–445.
48. Salustri A, Ulisse S, Yanagishita M, Hascall VC. Hyaluronic acid synthesis by mural granulosa cells and cumulus cells in vitro is selectively stimulated by a factor produced by oocytes and by transforming growth factor-beta. *J Biol Chem*. 1990;265: 19517–19523.
49. Petrey AC, de la Motte CA. Hyaluronan, a crucial regulator of inflammation. *Front Immunol*. 2014;5:101.
50. Wang A, de la Motte C, Lauer M, Hascall V. Hyaluronan matrices in pathobiological processes. *FEBS J*. 2011;278: 1412–1418.
51. Hascall V, Karamanos N. Regulatory roles of hyaluronan in health and disease. *FEBS J*. 2011;278:1411.
52. Ghatak S, Maytin EV, Mack JA, et al. Roles of proteoglycans and glycosaminoglycans in wound healing and fibrosis. *Int J Cell Biol*. 2015;2015:834893.
53. Baranova NS, Inforzato A, Briggs DC, et al. Incorporation of pentraxin 3 into hyaluronan matrices is tightly regulated and promotes matrix cross-linking. *J Biol Chem*. 2014;289:30481–30498.
54. Leali D, Inforzato A, Ronca R, et al. Long pentraxin 3/tumor necrosis factor-stimulated gene-6 interaction: a biological rheostat for fibroblast growth factor 2-mediated angiogenesis. *Arterioscler Thromb Vasc Biol*. 2012;32:696–703.
55. Inoue K, Kodama T, Daida H. Pentraxin 3: a novel biomarker for inflammatory cardiovascular disease. *Int J Vas Med*. 2012; 2012:657025.
56. Tseng SC, He H, Zhang S, Chen SY. Niche regulation of limbal epithelial stem cells: relationship between inflammation and regeneration. *Ocul Surf*. 2016;14:100–112.
57. Nguyen H, Rendl M, Fuchs E. Tcf3 governs stem cell features and represses cell fate determination in skin. *Cell*. 2006;127: 171–183.
58. Perl AK, Wert SE, Nagy A, Lobe CG, Whitsett JA. Early restriction of peripheral and proximal cell lineages during formation of the lung. *Proc Natl Acad Sci U S A*. 2002;99: 10482–10487.
59. Matsumoto K, Li Y, Jakuba C, et al. Conditional inactivation of Has2 reveals a crucial role for hyaluronan in skeletal growth, patterning, chondrocyte maturation and joint formation in the developing limb. *Development*. 2009;136:2825–2835.
60. Fulop C, Szanto S, Mukhopadhyay D, et al. Impaired cumulus mucification and female sterility in tumor necrosis factor-induced protein-6 deficient mice. *Development*. 2003;130: 2253–2261.
61. Kobayashi N, Miyoshi S, Mikami T, et al. Hyaluronan deficiency in tumor stroma impairs macrophage trafficking and tumor neovascularization. *Cancer Res*. 2010;70:7073–7083.
62. Bai KJ, Spicer AP, Mascarenhas MM, et al. The role of hyaluronan synthase 3 in ventilator-induced lung injury. *Am J Respir Crit Care Med*. 2005;172:92–98.
63. Dai G, Freudenberger T, Zipper P, et al. Chronic ultraviolet B irradiation causes loss of hyaluronic acid from mouse dermis

Investigative Ophthalmology & Visual Science

because of down-regulation of hyaluronic acid synthases. *Am J Pathol*. 2007;171:1451–1461.

64. Coulson-Thomas VJ, Caterson B, Kao WW. Transplantation of human umbilical mesenchymal stem cells cures the corneal defects of mucopolysaccharidosis VII mice. *Stem Cell*. 2013; 31:2116–2126.
65. Torihashi S, Ho M, Kawakubo Y, et al. Acute and temporal expression of tumor necrosis factor (TNF)-alpha-stimulated gene 6 product, TSG6, in mesenchymal stem cells creates microenvironments required for their successful transplantation into muscle tissue. *J Biol Chem*. 2015;290:22771–22781.
66. Farwick M, Gauglitz G, Pavicic T, et al. Fifty-kDa hyaluronic acid upregulates some epidermal genes without changing TNF-alpha expression in reconstituted epidermis. *Skin Pharmacol Physiol*. 2011;24:210–217.
67. Kouvidi K, Berdiaki A, Nikitovic D, et al. Role of receptor for hyaluronic acid-mediated motility (RHAMM) in low molecular weight hyaluronan (LMWHA)-mediated fibrosarcoma cell adhesion. *J Biol Chem*. 2011;286:38509–38520.
68. Mahoney DJ, Aplin RT, Calabro A, Hascall VC, Day AJ. Novel methods for the preparation and characterization of hyaluronan oligosaccharides of defined length. *Glycobiology*. 2001; 11:1025–1033.
69. Siiskonen H, Oikari S, Pasonen-Seppanen S, Rilla K. Hyaluronan synthase 1: a mysterious enzyme with unexpected functions. *Front Immunol*. 2015;6:43.
70. Cyphert JM, Trempus CS, Garantziotis S. Size matters: molecular weight specificity of hyaluronan effects in cell biology. *Int J Cell Biol*. 2015;2015:563818.
71. Dong Y, Pang Y, Li Q. The anti-tumor mechanisms in long-lived rodents [in Chinese]. *Yi Chuan*. 2016;38:411–417.
72. Triggs-Raine B, Natowicz MR. Biology of hyaluronan: insights from genetic disorders of hyaluronan metabolism. *World J Biol Chem*. 2015;6:110–120.
73. Fisher GJ. Cancer resistance, high molecular weight hyaluronic acid, and longevity. *J Cell Commun Signal*. 2015;9:91–92.
74. Tian X, Azpurua J, Hine C, et al. High-molecular-mass hyaluronan mediates the cancer resistance of the naked mole rat. *Nature*. 2013;499:346–349.
75. Faulkes CG, Davies KT, Rossiter SJ, Bennett NC. Molecular evolution of the hyaluronan synthase 2 gene in mammals: implications for adaptations to the subterranean niche and cancer resistance. *Biol Lett*. 2015;11:20150185.
76. Keane M, Craig T, Alfoldi J, et al. The Naked Mole Rat Genome Resource: facilitating analyses of cancer and longevity-related adaptations. *Bioinformatics*. 2014;30:3558–3560.
77. Tien JY, Spicer AP. Three vertebrate hyaluronan synthases are expressed during mouse development in distinct spatial and temporal patterns. *Dev Dynam*. 2005;233:130–141.
78. Mort RL, Douvaras P, Morley SD, et al. Stem cells and corneal epithelial maintenance: insights from the mouse and other animal models. *Results Probl Cell Differ*. 2012;55:357–394.
79. Secker GA, Daniels JT. Limbal epithelial stem cells of the cornea. *StemBook*. Cambridge, MA; 2008.
80. Albert R, Vereb Z, Csomos K, et al. Cultivation and characterization of cornea limbal epithelial stem cells on lens capsule in animal material-free medium. *PLoS One*. 2012;7: e47187.
81. Haddad A. Renewal of the rabbit corneal epithelium as investigated by autoradiography after intravitreal injection of 3H-thymidine. *Cornea*. 2000;19:378–383.
82. Huang AJ, Tseng SC. Corneal epithelial wound healing in the absence of limbal epithelium. *Invest Ophthalmol Vis Sci*. 1991;32:96–105.
83. Majo F, Rochat A, Nicolas M, Jaoude GA, Barrandon Y. Oligopotent stem cells are distributed throughout the mammalian ocular surface. *Nature*. 2008;456:250–254.
84. Buck RC. Cell migration in repair of mouse corneal epithelium. *Invest Ophthalmol Vis Sci*. 1979;18:767–784.
85. He H, Li W, Tseng DY, et al. Biochemical characterization and function of complexes formed by hyaluronan and the heavy chains of inter-alpha-inhibitor (HC*HA) purified from extracts of human amniotic membrane. *J Biol Chem*. 2009;284: 20136–20146.
86. He H, Tan Y, Duffort S, Perez VL, Tseng SC. In vivo downregulation of innate and adaptive immune responses in corneal allograft rejection by HC-HA/PTX3 complex purified from amniotic membrane. *Invest Ophthalmol Vis Sci*. 2014;55:1647–1656.